
**Science Arts & Métiers (SAM)**

is an open access repository that collects the work of Arts et Métiers Institute of Technology researchers and makes it freely available over the web where possible.

This is an author-deposited version published in: https://sam.ensam.eu
Handle ID: .http://hdl.handle.net/10985/21765

**To cite this version :**

Mohammad AHMADIFAR, Mohammadali SHIRINBAYAN, Khaled BENFRIHA, Abbas TCHARKHTCHI - Additive Manufacturing of Polymer-Based Composites Using Fused Filament Fabrication (FFF): a Review - Applied Composite Materials - Vol. 28, n°5, p.1335-1380 - 2021

Any correspondence concerning this service should be sent to the repository Administrator : scienceouverte@ensam.eu

Arts et Métiers Institute of Technology

https://doi.org/10.1007/s10443-021-09933-8

# Additive Manufacturing of Polymer-Based Composites Using Fused Filament Fabrication (FFF): a Review

**M. Ahmadifar[1,2] · K. Benfriha[2] · M. Shirinbayan[1] · A. Tcharkhtchi[1]**

**Abstract**
In this review paper, recent developments in the Fused Filament Fabrication (FFF) approach are provided for composite materials. Influencing parameters in FFF process such as road width, print speed, layer thickness, feed rate and build temperature of the model (both liquefier and envelope temperature), fiber orientation, the layer position, volume fraction, and infill orientation have been studied. These considered parameters in the strength/bonding or physicochemical characterizations of FFF-fabricated parts have been presented in detail. An overview of the mechanical properties of printed parts for different composite material systems is presented and discussed. Three types of reinforced polymers in FFF process have been considered: filled reinforced polymers, continuous fiber-reinforced polymers, and short fiber reinforced polymers.

**Keywords** Fused Filament Fabrication · Composite · Continuous fiber · Short fiber

## 1 Introduction

In recent years, a new stereo-lithography process has been developed to produce complex shapes. The main mechanism of the process was based on the 3-D design of a thin layer from the liquid polymer by using a laser beam. The final product was based on a layer of hardened resin having the same shape and dimension, which has been already generated by a computer-generated slice. The production of this kind of shape was then named rapid prototyping (RP) [1].

✉ M. Ahmadifar
mohammad.ahmadifar@ensam.eu

✉ M. Shirinbayan
mohammadali.shirinbayan@ensam.eu

K. Benfriha
khaled.benfriha@ensam.eu

A. Tcharkhtchi
abbas.tcharkhtchi@ensam.eu

[1] Arts Et Metiers Institute of Technology, CNAM, PIMM, HESAM University, 75013 Paris, France

[2] Arts Et Metiers Institute of Technology, CNAM, LCPI, HESAM University, 75013 Paris, France

Rapid prototyping (RP) is a generic term for several technologies in which components are fabricated without the requirement for conventional tooling. The use of these technologies allows for the automatic construction of physical objects from computer geometric models and permits quick production of prototypes, and thus substantially reduces product development time. Conventional milling and turning are good examples of subtractive processes. In contrast, RP techniques are additive processes and RP components are build-up gradually in layers. In RP, a computer-aided design (CAD) file of an object is converted into a physical model using a variety of manufacturing techniques [2, 3].

These technologies are commonly referred to as solid freeform fabrication (SFF) methods. SFF has become very successful in the marketplace in the past 3 decades [2]. The most popular SFF technologies to date are as follows: Stereo-lithography (SL), Laminated object manufacturing (LOM), Fused Filament Fabrication (FFF), Selective laser sintering (SLS), and Multi-jet modeling (MJM) [2, 3].

In addition, the number of different materials that can be employed in each process has increased significantly, improving the precision and functionality of the end products. Therefore, RP techniques are now worthy of consideration as alternative methods of the direct production of parts, components, or models for use in manufacturing processes [4].

Additive Manufacturing (AM) technologies offer the potential for significant cost savings due to reduced material waste and the capability for a tool-less production of intricate geometries. Therefore, they have gained considerable attention during the last decade. The Fused Filament Fabrication (FFF) process, which is also termed Fused Deposition Modeling (FDM), is one of the most popular AM methods for manufacturing the parts by polymer or composite materials. This process utilizes a continuous filament of a thermoplastic material as raw material. The molten raw material extrudes from the print head, then deposits on the build platform layer by layer. Which caused the formation of the designed and required part(s) [4].

The Fused Filament Fabrication (FFF) process is the main objective of this paper. FFF process typically begins with a solid model of the planned part as generated in a CAD system. This model is oriented in the desired build direction and post-processed within the CAD system into a stereolithography format (STL). The STL representation is then decomposed into horizontal layers representing thin cross-sections of the product. Solid models for these structures are then defined and sliced similarly. Actual instruction codes for the FFF machine are then generated and include a path plan for each layer of the sliced model [4]. The only required post-processing activity is the removal of the support structures.

Fused Filament Fabrication (FFF), first developed by Stratays Inc [4], USA, is a solid freeform fabrication process. It forms three-dimensional objects from computer-generated solid or surface models. An FFF machine is a computer numerically controlled (CNC) machine, carrying extruder nozzles. A spool of modeling filament feeds the one head, and a spool of support material feeds the other. The machine fabricates prototypes by extruding the filament through a heated nozzle in a prescribed pattern onto a platform (Fig. 1). As the material is deposited, it cools, solidifies, and bonds with the surrounding material. At the end of each finished layer, the base platform is lowered in preparation for the deposition of the next layer. The deposition path and parameters for every layer are chosen depending on the material used, the fabrication conditions, and the applications of the designed part, and the preferences of the designer.

The most common materials employed in the FFF process could be classified as follows: Polylactic acid (PLA), Investment casting wax, Acrylonitrile butadiene styrene (ABS), Polycarbonate (PC), Polyphenylsulfone (PPSF), Polypropylene (PP), Polyethylene (PE), Polyether ether Ketone (PEEK), Nylon (PA), etc. These polymers may be filled with

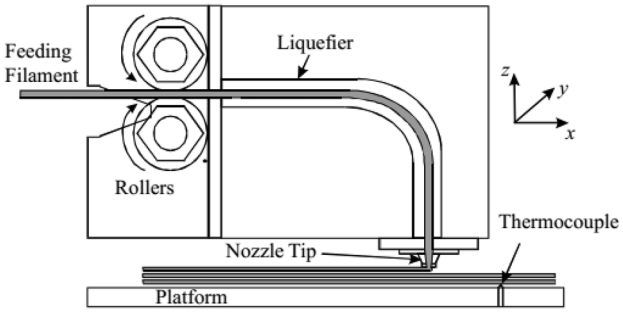


**Fig. 1** Schematic of FFF process [4]

different types of fillers like talc, mica, wollastonite, calcium carbonate, mineral pigments, carbon black, and micro-glass marble. It could be also reinforced by the continuous or discontinuous glass or carbon fibers to produce the composite material [4].

The materials are selected based on their thermo-physical and mechanical characteristics. Key mechanical properties of an FFF material include strength, stiffness, and ductility [5]. The other requirements on thermo-physical properties include the low coefficient of thermal expansion, minimal shrinkage, high heat resistance, no/few volatile molecules, and no phase transformation in the solid-state. Lower thermal expansion is essential to achieve dimensional accuracy and stability of the part. The amount of linear shrinkage in a part between the building temperature and the end-use temperature should be less than 1%.

Rheological and thermal properties are also taken into consideration in the material formulation and selection [4]. Relatively low melt viscosity is required for the material to flow through the nozzle. It is therefore necessary to increase the temperature to obtain a low viscosity. However, this increase in temperature is limited due to the low thermal stability and the degradation of the polymer. In the FFF process, several parameters can influence the process with different degrees of influence. Therefore, the optimization of all these parameters is necessary to allow a good adhesion between each layer with the layer previously deposited.

To be able to make a part with the FFF process, the polymer must be in the molten state with low viscosity. This condition limits the area of the process. The viscosity of polymer depends on its molecular weight and temperature. The temperature-molar mass diagram of the polymer allows knowing the process area of a polymer (Fig. 2). On this diagram, the different zones correspond to the different physical states of the polymer:

- Zone I: solid-state.
- Zone II: Rubbery state.
- Zone III: liquid/viscous state.
- Zone IV: zone of degradation. Zones are separated by transition temperatures:

$M_C$ ($\approx$ 5 kg/mol) is the critical molecular weight.
$T_g$: glass transition temperature (relative to the amorphous phase).
$T_f$: melting point related to the crystalline phase.
$T_D$: degradation temperature of the polymer: from this border, the polymer begins to degrade.

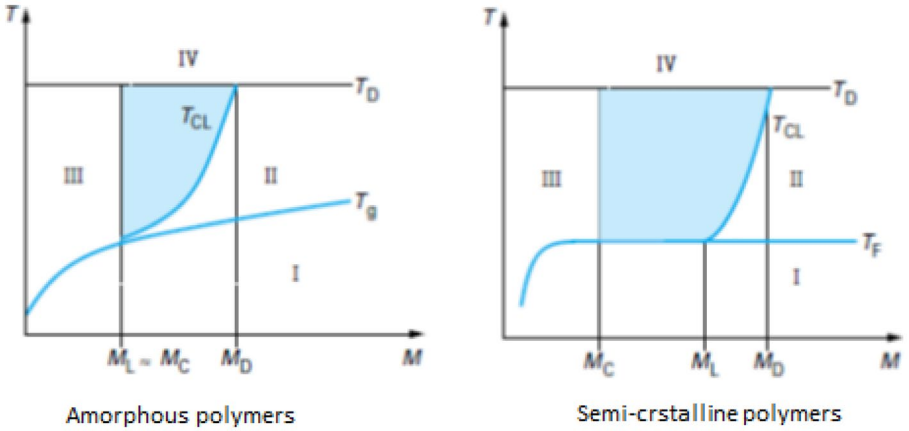


**Fig. 2** Temperature-Molecular Weight diagram of thermoplastic polymers

$T_{CL}$: transition temperature rubber / liquid state. This last temperature has essentially technological signification. It is the temperature below which material is too viscous to be used. The process temperature must be always higher than $T_{CL}$.

In the FFF process, the molten polymer in the extruder passes through the cylinder, and the molten filament will be deposited onto the previous one (according to Fig. 1) that is in the progress of cooling and causes the re-heating of this last one [6, 7]. Because of the cyclic temperature profile of each layer during deposition, the key point that affects the bonding of two adjacent filaments would be the optimization of the temperature profile.

The manufacturing capabilities of complex geometries and low manufacturing costs have motivated researchers to undertake various studies for improving the behavior of parts manufactured by the Fused Filament Manufacturing (FFF) process [8, 9]. Despite the mentioned advantages, in comparison to the conventional methods [1], mechanical properties of parts manufactured by the FFF process are inherently poor and there is a limited number of researches in this regard [10, 11].

To have a better understanding of the features of temperature profiles between adjacent filaments, various mathematical approaches have been proposed. A transient heat transfer analysis for the filament deposition with physical contacts between any filament and its neighbors has been proposed [2]. Also, a 2D heat transfer model of two-filament was generated to consider the temperature evolution during FFF process deposition using Finite Element Method (FEM) [3]. Furthermore, a 1D transient heat transfer model was developed by Q. Sun [4] and combined with the spherical particle sintering model (O. Pokluda et al. [4]) to estimate the FFF temperature profile and the bond formation for a single filament depositing process [4].

In this review paper, process parameters, and experimental works in the case of composite materials obtained by the FFF process will be reviewed. Different experimental characterization results are presented. This research helps design and optimize the processing parameters to improve the mechanical properties of composite products fabricated by FFF. Control of these parameters allows designers to better adapt the mechanical characteristics of composite parts to their usage.

## 2 FFF influencing parameters

The manufacturing of the parts depends on many parameters related to the following elements: Material, shape and geometry, process, and tools (mold, machine, and …). Numerous studies focused on finding a relationship between the properties and processing parameters of FFF process in printed parts, such as layer thickness or raster angle [10, 12, and 13]. In FFF process, each parameter has its own influence on the microstructure and bonding/strength of the fabricated parts. Some process parameters have been introduced in Fig. 3.

Due to the nature of FFF, almost all the 3D-printing machines comprise numerous process parameters. This allows users to utilize a wide range of parameters. Following Fig. 3, process parameters such as road width, print speed, layer thickness, feed rate and build temperature of the model (both liquefier and envelope temperature), fiber orientation, the layer position, volume fraction, infill orientation contribute to be considered and taken into account in the strength/bonding or physicochemical characterizations of FFF-fabricated parts. Almost all of them affect the filament bonding and consequently the mechanical behavior of 3D-printed parts. However, researchers tried to focus on some key parameters due to the numerous values that exist for the FFF process by optimizing the experimental procedure to obtain the best combination of parameters that help to improve the bonding of adjacent filaments, as much as possible. The development of the mechanical behavior and dimension accuracy of the printed parts in comparison with the desired dimension values are considered as the criteria of the suitable combination of the process parameters, as optimized additive manufacturing procedure.

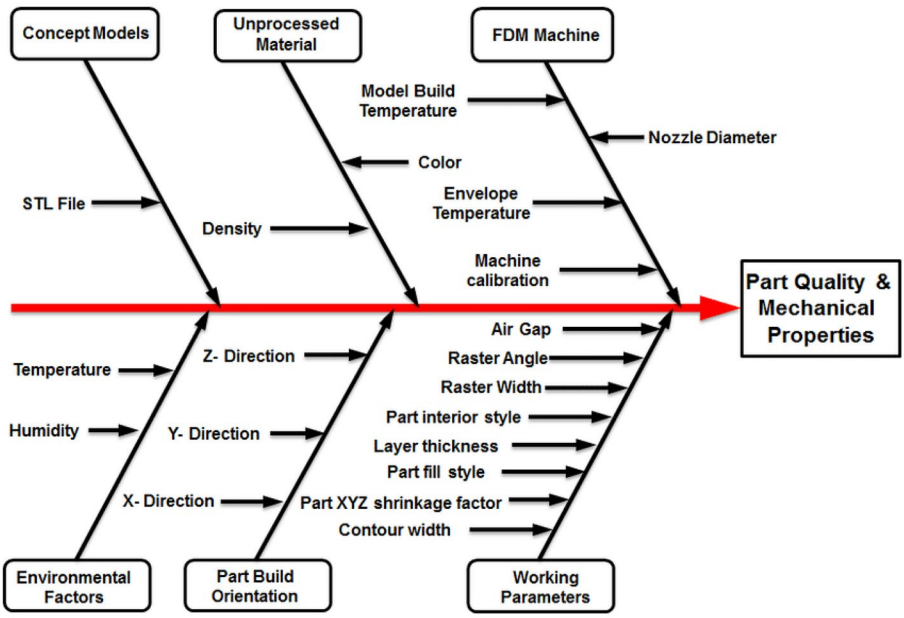


**Fig. 3** Representation of influencing parameters in FFF process [5]

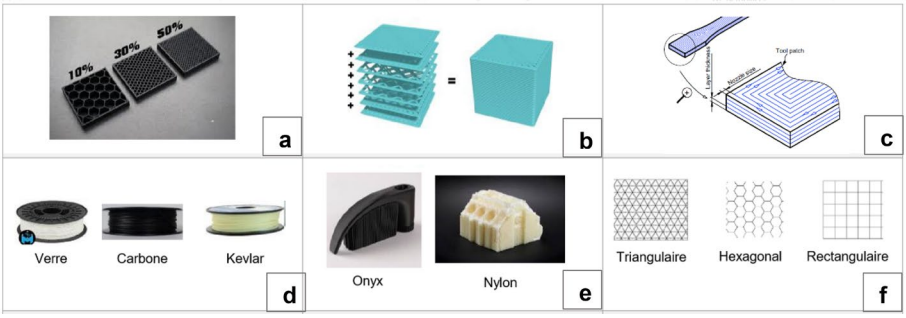


**Fig. 4** FFF parameters in composites, (**a**) Effect of infill density, (**b**) Effect of the quantity of the layers, (**c**) Effects of tool path, nozzle size, and layer thickness, (**d**) Effect of the type of the used reinforcement material, (**e**) Effect of the type of the used matrix, (**f**) Effect of infill pattern

Various research exists on the consideration of the influence of parameters on parts fabricated using FFF. Build orientation and raster angle and their effects on the mechanical properties of 3D-printed parts have been consequently studied and they have tried to analyze the effect of raster angle by consideration of infill patterns (Fig. 4) [10, 12].

Regarding the type of applied material and the studied parameters, it was found that almost all researchers tried to consider the effect of parameters by the different methods of characterization (e.g. tensile or bending).

## 3 FFF process in polymers

The effect of in-process and post-process thermal treatment and the environment temperature or envelope temperature on the fabricated parts have been studied. Based on Fig. 5, diffusion, and neck-growth between of two adjacent filaments would be affected

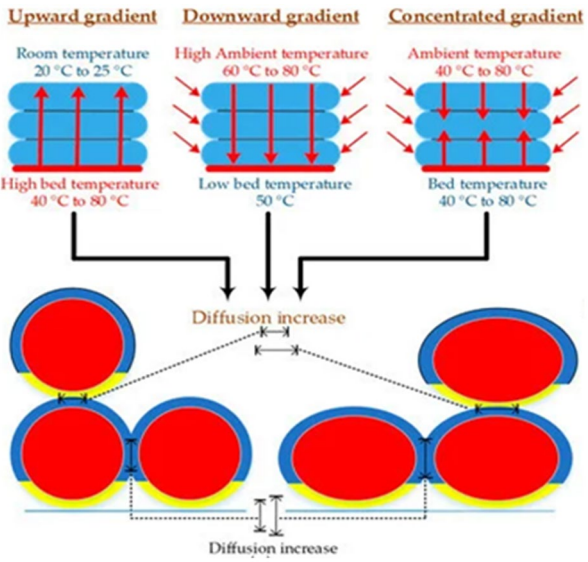


**Fig. 5** In-process thermal treatment at the different type of heat gradient on printed structure [14]

by changing of environment or envelope temperature in which it approves the importance of heat transfer in this process.

Table 1 presents an overview of FFF process parameters for polymers without any reinforcements. One can note that these studies can be useful for the understanding of FFF process in composite especially the effect of reinforcements to improve mechanical properties of structures. In fact, in this table different research works have been reviewed to show their importance. In these studies, some processing parameters such as raster, air gap, raster width, layer thickness, temperature, building orientation, etc. have been analyzed. The results of all studied to confirm the importance of temperature and building orientation effects on the mechanical properties of the printed sample. However, as mentioned this information could help us to better study the bonding filaments and consequently mechanical properties of composite parts made by the FFF process.

**Table 1** FFF process in polymers

| Study | Materials | Parameters |
|---|---|---|
| Fodran [15] | ABS | Fill gap, line width, slice thickness |
| Bertoldi [6] | ABS | Building orientation, raster orientation |
| Es-said [16] | ABS | Layer orientations |
| Rodriguez [17] | ABS | Fiber gap, flow rate |
| Ahn [18] | ABS | Raster orientation, bead width, color, temperature |
| Lee [7] | ABS | Raster, air gap, raster width, layer thickness |
| Sun [8] | ABS | Temperature variations with part building location |
| Sood [9] | ABS | Layer thickness, orientation, raster angle, and air gap |
| Fatimatuzahraa [10] | ABS | Raster (axial, crisscross, cross, and transverse) |
| Sood [19] | ABS | Layer thickness, orientation, raster angle, air gap |
| Croccolo [11] | ABS | Raster pattern, building orientation |
| Durgun [1] | ABS | Raster angles, building orientation |
| Gorsky [2] | ABS | Building orientation |
| Baich [3] | ABS | Infill (low, high, double dense, solid) |
| Gorski [4] | ABS | Orientation |
| Ziemian [20] | ABS | Raster orientations |
| Onwubolu [21] | ABS | Layer thickness, orientation, raster angle, and air gap |
| Tymark [22] | ABS, PLA | Layer thickness, raster orientation |
| Ebel [23] | ABS, PLA | Infill pattern, infill percentage |
| Rankouhi [24] | ABS | Layer thickness, raster orientations |
| Letcher [25] | ABS | Number of layers, raster orientation |
| Fernandez [26] | ABS | Infill, fill pattern |
| Alvarez, 2016 [27] | ABS | Infill |
| Hernandez [28] | ABS | Building orientations |
| Torrado [29] | ABS | Raster patterns |
| Mahmood [12] | ABS | Width, thickness, infill density, no. of shells |
| Ransey [13] | ABS | Building orientations, infill |
| Tanikella [14] | Nylon, ABS, PC | Different materials, color, building orientation |
| Cantrell [30] | ABS, PC | Raster, building orientations |

## 4 FFF process in polymer-based composites

### 4.1 Powder reinforced polymers

Nikzad, et al. [31], used three types of materials as the development of the new powder reinforced composite materials by the FFF process. The main reason for using powder as a reinforcement (filler) is to improve the electrical properties and thermal conduction (using metals powders). The powders, which were utilized as reinforcement (filler) for improving the electrical or thermal conduction, often reduce the strength of the materials. Therefore, they are not often considered as mechanical reinforcements in polymer composite materials.

The first used material was Acrylonitrile Butadiene Styrene (ABS) thermoplastic, as the matrix. Other used ones were two composites used as feedstock materials, which were copper powder mixed in ABS matrix and another one was iron powder mixed in ABS matrix. According to characterize the related viscoelastic properties of these developed composites materials as feedstock in the FFF process, Dynamic Mechanical Analysis (DMA) technique has been used. The varying volume fractions of metal powders (5%, 10%, 20%, 30%, and 40%) were used according to produce the appropriate feedstock filament. The related shape of the used powder particles was spherical for copper and irregular for iron. The purity of both used powder (copper and iron) was 99.7% with two particle sizes of 10 μm and 45 μm for copper and one particle size of 45 μm for iron powders (Table. 2).

Figure 6(a) is related to the variation of the measured thermal conductivity of the copper composites of the large used particle sizes with different copper content at different temperatures. According to Fig. 6, the observed temperature increase had a negligible influence. However, in the case of sample B4, which was related to the high concentration of the copper particles (30 vol. %), an obvious thermal conductivity increase, above the glass transition temperature of the matrix was observed. The increase of the particle's mobility at the beyond the temperature of the matrix glass transition was reported as the reason.

The lower concentration of the copper particles up to the volume fraction of 10% (samples B1 and B2), could not useful, according to improve the thermal resistance of the ABS matrix. In the case of the volume fraction of 20%, the conductive chains of the

**Table 2** Metal/polymer composites constituents [31]

| Composite designation | Matrix | Metal filler type | Filler size (μm) | Filler loading (%) |
|---|---|---|---|---|
| A1 | ABS | Cu | 10 | 5 |
| A2 | ABS | Cu | 10 | 10 |
| A3 | ABS | Cu | 10 | 20 |
| A4 | ABS | Cu | 10 | 30 |
| A5 | ABS | Cu | 10 | 40 |
| B1 | ABS | Cu | 45 | 5 |
| B2 | ABS | Cu | 45 | 10 |
| B3 | ABS | Cu | 45 | 20 |
| B4 | ABS | Cu | 45 | 30 |
| B5 | ABS | Cu | 45 | 40 |
| C1 | ABS | Fe | 45 | 5 |
| C2 | ABS | Fe | 45 | 10 |
| C3 | ABS | Fe | 45 | 20 |
| C4 | ABS | Fe | 45 | 30 |
| C5 | ABS | Fe | 45 | 40 |

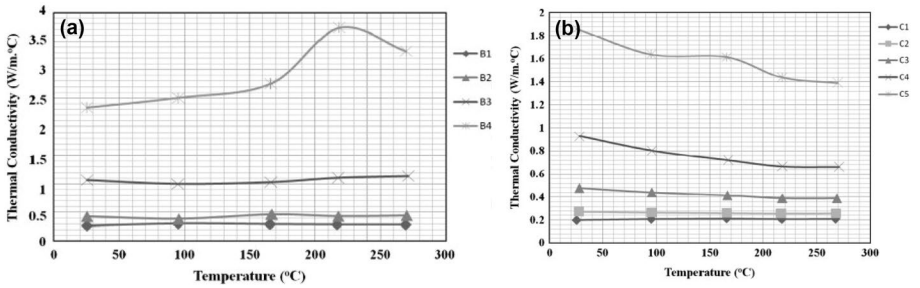


**Fig. 6** Thermal conductivity of (**a**) copper-filled ABS and (**b**) iron-filled ABS composites at various temperatures [31]

copper were formed. In the other words, the volume fraction of the 20% copper powders was required to achieve a percolation concentration. This formation and its related effect on the thermal resistance were more tangible in the case of 30% volume fraction. As for the reason, easier mobilization thanks to the matrix state change from the solid to the liquid state at the above glass-transition temperature of the matrix.

According to Fig. 6(b), as the comparison of the effect of the iron and copper as the used reinforcements of the ABS matrix on the thermal conductivity of the fabricated composites, it was clear that the iron particles had lower influence. The effect of iron particles was sensible when the related particle concentration reached the 30% volume fraction (sample C4).

Figure 7(a) is related to the dynamic mechanical result of the ABS reinforced by the used finer copper particle size. It was observed that below the glass-transition temperature, as the volume fraction of the used filler was increased, the storage modulus of the composite was increased, too. The trend was continued up to 30% of the filler volume fraction (sample A4). Nevertheless, the storage modulus of the composite was decreased as the volume fraction of the filler was increased by more than 30%. The agglomeration of the used reinforcement particles (sample A5) and accumulating of the voids have been stated as reasons for the weakening of the ABS matrix by the used finer copper particles, instead of strengthening the matrix.

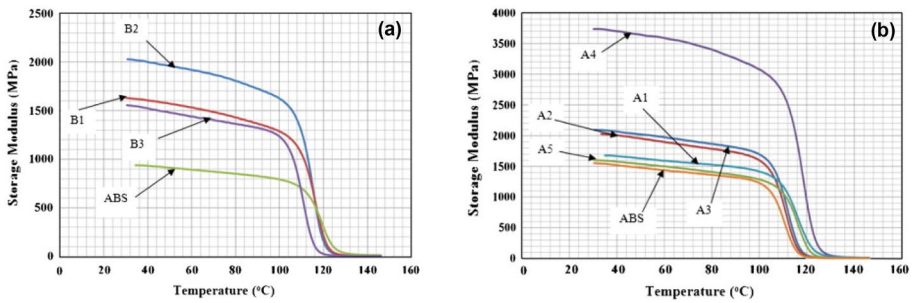


**Fig. 7** The storage modulus of various Copper/ABS composites with the copper particle size of (**a**) 10 nm and (**b**) 40 nm at the different temperature values [31]

Figure 7(b) shows the dynamic mechanical result of the ABS reinforced by the used coarser copper particle size. The storage modulus of the composite was increased as the volume fraction of the filler was increased up to 10%. However, the stated trend was inverted as the filler fraction was increased more than 10%. The weaker interlock of the filler matrix and the inappropriate distribution of the used fillers in the matrix were stated as the reason. In fact, the maximum achieved storage modulus in the case of the used larger copper particles was about 2GPa, while it was reported about 3.5-4GPa, in the case of the used finer copper particles as reinforcements.

Figure 8 presents the dynamic mechanical result of the ABS reinforced by the used iron particles. The effect of the iron particles was considered up to 30% volume fraction, which caused the range of the 2.5-3GPa as the storage modulus (stiffness) of the fabricated composite. The stiffness values of the Iron/ABS composites were higher in comparison with the same used particle size of the copper as reinforcement, under the 10–20% volume fraction condition of the fillers.

Hwang et al. [32] studied the thermo-mechanical properties of the developed metal/polymer composite and the printing parameter, by the FFF process. The used metal powders were copper and iron with the size of 24 μm and 34 μm, to reinforce the ABS matrix. The loading deal of the metal particles was varied to study the effects of the used metal powder on the mechanical behavior of the fabricated filament. It has been reported that by the increase of the metal content, the tensile strength of the specimens was decreased. As finding it reason, the microstructure of the cut plane of the printed specimens (ABS-CU composite) was observed (Fig. 9, 10). It was observed more voids in the case of the 30 Wt. % of the copper particles in comparison with the use of the 10 Wt. % of copper particles. These voids caused the lower bonding between the layers, then the lower tensile strength of the specimens with 30 Wt. % copper particles in comparison with specimens with 10 Wt.

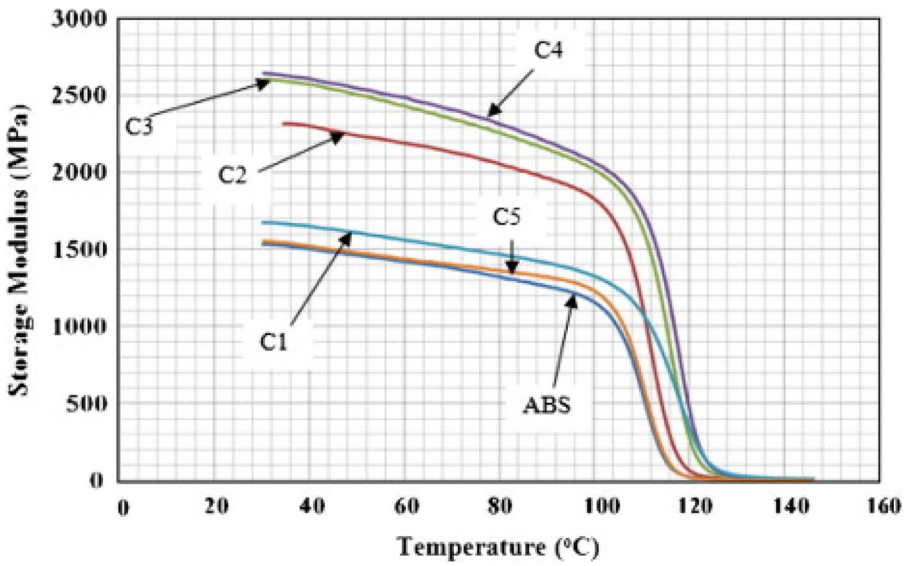


**Fig. 8** The storage modulus of various Iron/ABS composites with the iron particle size of 45 μm at the different temperature values [31]

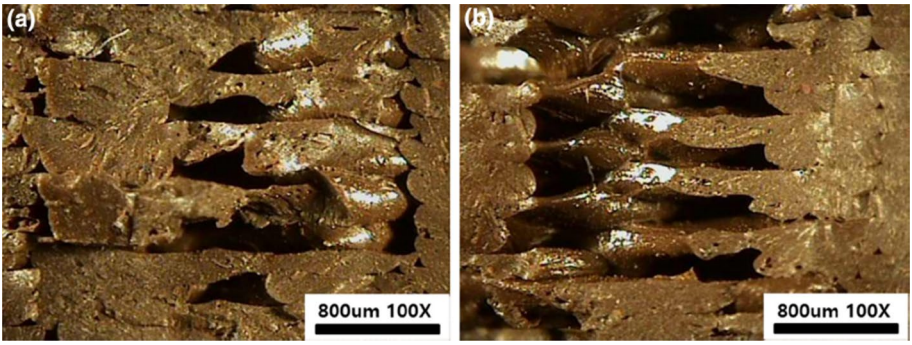


**Fig. 9** The microscopic structure of cutting plane of specimens: (**a**) ABS-Cu10 wt. % and (**b**) ABS-Cu30 wt. % [32]

% copper particles. In addition, the thermal conductivity of the prepared metal/polymer composite was progressed and improved by the increase of the metal content.

Isakov et al. [33], could improve the dielectric permittivity by adding $BaTiO_3$ and $CaTiO_3$ into the polymer matrix (ABS and PP) by the FFF process. Also, Shemelya et al. [34], could improve dielectric permittivity, X-ray attenuation factor, and impact resistance of PC (polymer matrix) by adding the Tungsten particles.

Boparai et al. [35] studied the tribological properties of the fabricated ABS and Nylon 6-Al-$Al_2O_3$, by the FFF method. As for tribology characterization, the wear test was carried out on the related FFF manufactured specimens with the dimensions of 10 mm as diameter and 30 mm as length. The wear test was performed following ASTM G 99 standard at room temperature. This research illustrated that the use of Al and $Al_2O_3$ as fillers could develop the wear properties, by comparison of the printed Nylon 6-Al-$Al_2O_3$ and the printed ABS parts. The related particle size of the used Al and $Al_2O_3$ were 41–44 µm and 125–149 µm, respectively. As the tribological test, the different loads were applied during 5 and 10 min at 1.36 (m/s), as sliding velocity. In the case of the fabrication of the nylon 6-Al-$Al_2O_3$ up to 40% of the filler materials ($Al_2O_3$ and Al) were used, as the filler of the nylon 6 matrix.

Table 3 shows the composition of each printed type of the nylon 6-Al-$Al_2O_3$ composites and the respective MFI of each composition. Indeed, the rheological behavior of

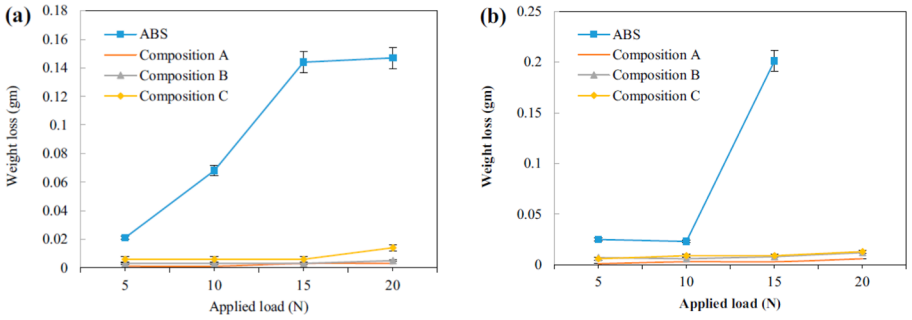


**Fig. 10** Material weight loss with applied load for (**a**) 5 min and (**b**) 10 min, obtained from tribology evaluations [35]

**Table 3** Weight proportion and MFI of different compositions [35]

| Composition | Nylon 6 | Al | $Al_2O_3$ | MFI |
|---|---|---|---|---|
| A | 60 | 26 | 14 | 2.19 |
| B | 60 | 28 | 12 | 2.25 |
| C | 60 | 30 | 10 | 2.31 |

composite material with consideration of temperature and viscosity within processing in the liquefier head section of FFF was studied employing the melt flow index (MFI) test. The MFI is introduced as an alternative measure of viscosity for comparative purpose. It is defined as the amount of the related polymer in 'gm' extruded in '10' min via a capillary of standard dimensions (diameter $2.0955 \pm 0.0051$ mm and length $8.0 \pm 0.025$ mm), according to ASTM D1238–73 standard.

It has been reported that the MFI values of each composite were decreased by the decrease of Al and the increase of $Al_2O_3$. The increase of the amount of the large particle size in the reinforced matrix was stated as the decrease of the MFI value.

In addition, it has been understood that as the content of $Al_2O_3$ in the printed composites was decreased, the related material loss to the wear was increased, according to Table 3.

It was stated that the ABS material had more friction force under all conditions, in comparison with composite ones. In fact, the presence of the $Al_2O_3$ in the reinforced nylon composites introduced such as the bearing, caused less material loss, too. So, because of the stated property of the existence of $Al_2O_3$ particles, the composition "A", had the lowest friction load in comparison with the other compositions (B and C), according to Fig. 11. Also, the printed composites had the lower friction coefficient in comparison with the fabricated ABS parts. It was observed that the friction coefficients of the composite materials were changed, slightly by varying the applied load and duration.

SEM observation revealed that in the case of the comparison between the printed nylon 6-Al-$Al_2O_3$ and ABS parts, the composite ones had higher wear resistance, thermal stability, and stiffness (Fig. 12).

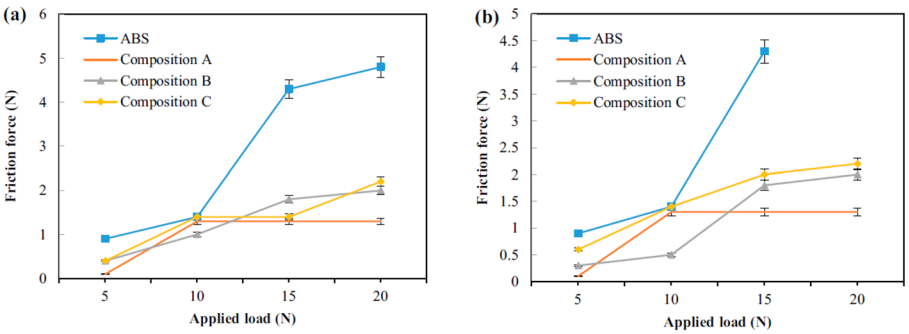


**Fig. 11** Obtained curves related to friction force with applied load for (**a**) 5 min and (**b**) 10 min on ABS, nylon 6–26 Al-14 $Al_2O_3$ (composite A), nylon 6–28 Al-12 $Al_2O_3$ (composite B), and nylon 6–30 Al-10 $Al_2O_3$ (composite C), from tribology evaluations [35]

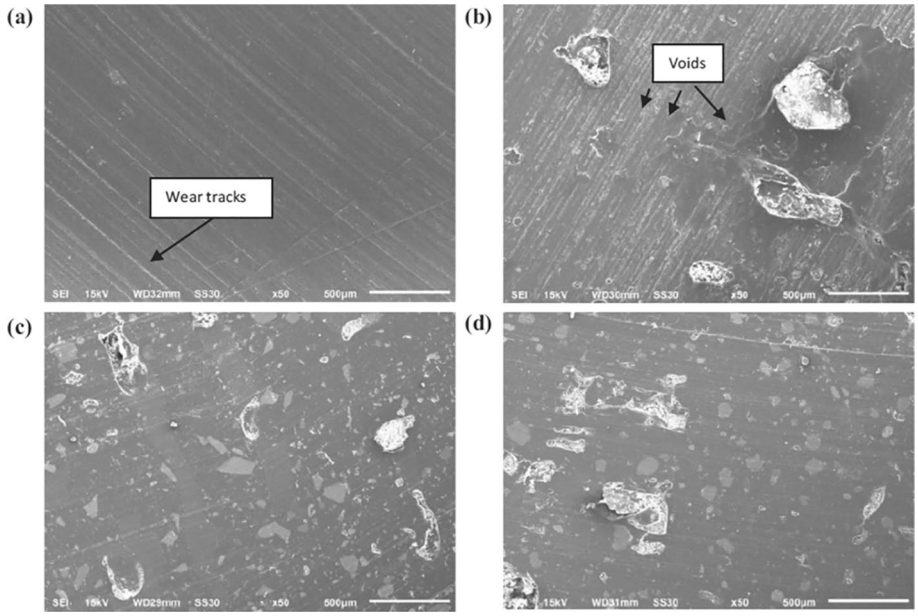


**Fig. 12** SEM images of (**a**) ABS material, (**b**) composition 'A', (**c**) composition 'B' and (**d**) composition 'C', obtained from tribological observations [35]

## 4.2 Fused filament fabrication of fiber-reinforced polymers

### 4.2.1 Continuous fiber-reinforced polymers

The strength of polymeric composites is mainly dependent on their two important components, which are the polymer matrix and the used reinforcement(s). In fact, the strength of polymeric composites, mainly originates from two aspects. First, the individual consideration, which is the strength of polymer matrix side and used reinforcement(s) side, separately. The second aspect is the related consideration of the collaboration of these two components, in the unique manufactured materials as composites, such as their adhesion. Between the two stated considerations, the second one sometimes is possible to be manipulated. In the case of the used 3D printer, which have one nozzle, different methods according to increase the impregnation of the fibers have been reported such below:

- Heating the fibers before entering to the nozzle, to increase the permeation of polymer [36].
- Heating of the used polymer (matrix) and passing the reinforcement through the polymer matrix, which has been in the molten state [37].
- Modification of the fibers by chemical solution before the feeding (sizing agent) [38].
- Printing without any heating and modification of the used fibers [39].

Matsuzaki et al. have studied the manufacturing of the PLA-continuous carbon composite by FFF. They have heated the fiber for fusing the fiber surface with polymer

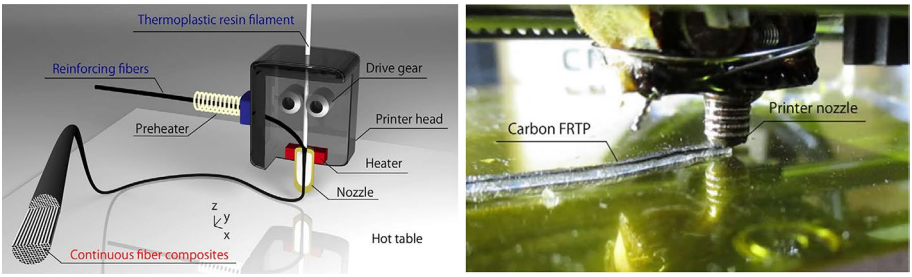


**Fig. 13** Schematic of the 3D printer head used to produce continuous FRTPs using in-nozzle (Left) and photograph of the 3D printing of a CFRTP (Right) [36]

matrix in synchronized fiber and polymer filament feeding (one-nozzle 3D printing machine), according to Fig. 13. In fact, the used fibers have been heated before entering the nozzle, by nichrome wire. It has enhanced the infiltration and permeation of the carbon fiber bundle with used PLA resin. The heat has diffused to the resin, decreased viscosity of the PLA, and caused the increase in the tensile strength [36].

Haoa et al. [37] studied the continuous carbon fiber reinforced thermosetting composites by FFF. An epoxy resin (E-54(616)) was utilized as the thermosetting matrix material; also as for reinforcement, a carbon fiber bundle (HF10, 3000 fibers in a bundle) was applied. It is stated that the high costs related to manufacturing of the continuous carbon fiber reinforced thermosetting composites restrict their use in the automotive industries, but these materials have a wide application in astronautics and aeronautics, thanks to their special properties and behaviors, such as good corrosion resistance, good fatigue behavior, high specific stiffness, and high specific strength [40]. Therefore, the approaching of the new low-cost methods of manufacturing of these composite structures will attract the industrials' attention. The used method was proceeding the fiber bundle through the pool of epoxy and then entering the printing head. After printing onto the building platform, the specimens were cured in high-temperature chamber. The composites lamina, honeycomb, and grid were manufactured, as was stated, according to Fig. 14.

Finally, the tensile and three-point bending behaviors of the printed composite lamina were characterized, therefore the fiber orientation of the three-point bending and tensile tested specimens were according to the lamina pattern (Fig. 14(a)). The dimensions of the printed samples for the stated mechanical tests were 250 mm × 25 mm × 3 mm. The

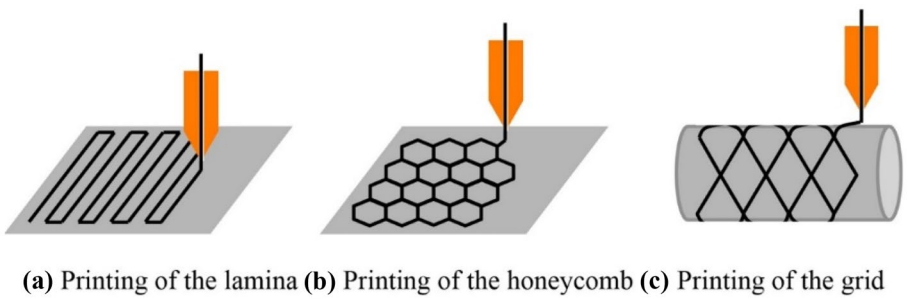


**Fig. 14** Scheme for the printing process [37]

flexural strength and elastic modulus were 202 MPa and 143.9 GPa, respectively. In addition, the tensile strength and elastic modulus were 792.8 MPa and 161.4 GPa. These results were compared with similar printed reinforced thermoplastic composites and printed short carbon fiber reinforced thermosetting composites. The failure mechanism of the printed composite lamina was studied. The failure was started by in-plane matrix cracking. Then, the crack has expanded with an increase in the applied load. Eventually, the separation of the layers occurred, and the fiber and the matrix were debonded, which caused partial fiber breakage. The fractography of the printed continuous carbon fiber reinforced thermosetting composite lamina specimens were performed after tensile and three-point bending tests. The fractography was done by use of SEM observation of the fractured cross-section of the tested specimens (Fig. 15). The fiber breakage was started as the related dominant failure mode of the fiber-reinforced thermosetting composites. However, the fiber pull-out was stated as the dominant failure mode of the manufactured reinforced thermoplastic composites by 3D printing (according to [38]).

In another study, Akhundi et al. studied the manufacturing of the PLA-continuous fiber (here, glass fiber yarn) composite part by FFF. In fact, the continuous glass fiber yarn entered polymer, which were molten in the nozzle, so the yarn was coated and partially impregnated with molten used PLA, as has been stated. It was concluded that the mechanical properties of produced composite by FFF was depended on the fiber volume content. It was noted that it is important to maximize the content of the fiber-volume to produce the composite part with high strength and modulus and then, to increase the accuracy of the prediction of the printed composite [41].

Nanya Li et al. [38] applied modification on carbon fiber bundles, which were reinforcement components of produced composite by infiltration in PLA sizing agent before the printing as the manufacturing process, to improve the mechanical properties. In fact, the used 3D-printing machine was a one-nozzle setup (according to Fig. 16) and the applied approach for fiber impregnation was “Modification of the fibers by chemical solution, before the feeding”.

Printed samples under three different conditions, which were PLA, carbon fiber reinforced PLA and modified carbon fiber reinforced PLA were produced. Then, the printed samples were characterized by mechanical tests.

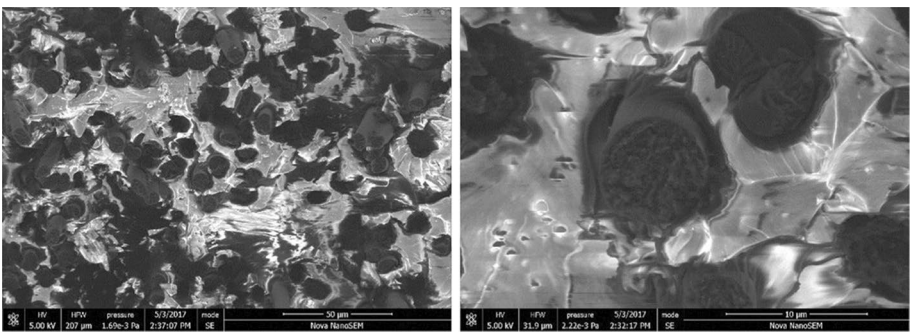


**Fig. 15** SEM images of the fractured cross-sections related to epoxy resin (E-54(616)) reinforced with continuous carbon fiber composites [37]

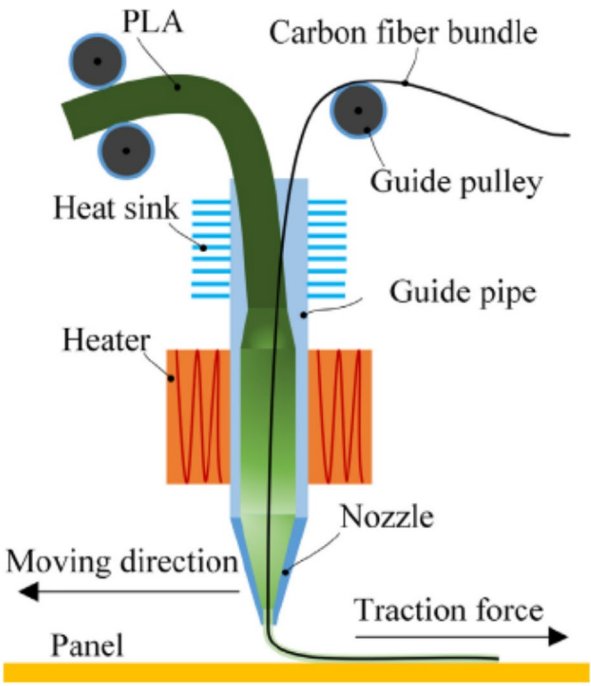


**Fig. 16** Schematic of the designed extrusion device to printing continuous carbon fiber reinforced PLA [38]

According to Table 4, the flexure strength of the original carbon fiber was so close to the PLA samples. But the modified carbon fibers showed more strength (about 164%) than the original composite. As a reason, it was stated that this observation could be attributed to the reason that the three-point bending test and flexural property is affected by interfacial strength between matrix and reinforcement, significantly. In addition, the tensile strengths of the two kinds of carbon fiber composite (with and without modification), were significantly more than PLA printed samples.

As the SEM observation, the microstructure of the original carbon fiber and modified carbon reinforced composites, before and after tensile test have been compared (Fig. 17). According to Fig. 17(a) and (b), the stronger interface and better wetting of carbon fibers by PLA resin, due to the applied modification was clear. According to Fig. 17(b), there are just small bridges between fibers (yellow circle), which transfer the loads between fibers. By the way, there were many voids between carbon fibers, which are representative of poor infiltration of PLA and fibers. On another hand, the higher infiltration and more bonding of matrix and modified carbon fiber are visible in Fig. 17(e). Finally, as for a comparison of the fractured surfaces of two kinds of original and modified composites (Fig. 17(e) and (f)), the complete coated fibers (cracked fibers) by PLA resin, were rare. On the contrary,

**Table 4** Statistic results of tensile and flexure strength of three different samples [38]

| Mechanical properties | PLA | Carbon fiber reinforced PLA | Modified carbon fiber reinforced PLA |
|---|---|---|---|
| Tensile strength (MPa) | 28 | 80 | 91 |
| Flexure strength (MPa) | 53 | 59 | 156 |

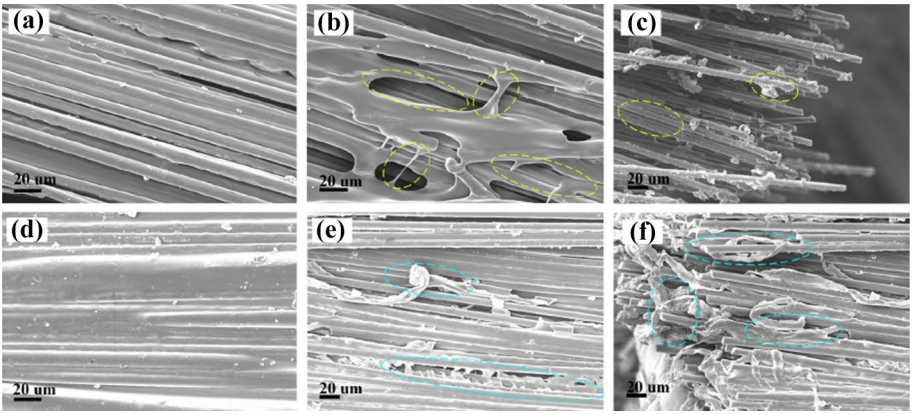


**Fig. 17** SEM micrographs of printed composites, (**a**) fiber-matrix interface of carbon fiber reinforced PLA specimen, (**b**) carbon fiber reinforced PLA specimen after tensile test, (**c**) fiber pull-out of the specimen after tensile test, (**d**) fiber-matrix interface of modified carbon fiber reinforced PLA specimen, (**e**) modified carbon fiber reinforced PLA specimen after tensile test and (**f**) fiber pull-out of modified carbon fiber reinforced PLA specimen after tensile test [38]

most of the carbon fibers were completely coated by PLA resin, and the significant separation of fiber and matrix was not observed. This observation has been stated as the reason for the remarkable difference in flexure strength of the original carbon fiber composite and modified ones, which were studied [38].

Tian et al. [39] studied the continuous carbon fiber reinforced PLA composites, in which the reinforcement and PLA filament have been fed into the FFF machine, simultaneously. They studied the five parameters, which have affected the pressure and temperature of the fabricated PLA composite. The chosen parameters were temperature of liquefier, layer thickness, feed rate of filament, hatch spacing (which was introduced as the central distance between two adjacent lines) transverse movement speed. As the parameters were changed, the mechanical performance of manufactured specimens was changed. The obtained flexural strength and modulus from the 3-point bending test, as the criteria of the mechanical properties, were considered to optimize the stated selected parameters of the process.

The study on the effect of liquefier temperature was done in the range of 180–240 °C, in which the melting flow index of PLA at the temperature of 180 °C and 240 °C, were measured 2 g/10 min and 36 g/10 min, respectively according to the Fig. 18.

The related results of the evolution of the flexural strength and modulus were reported in Fig. 19. Therefore, the flexural strength and modulus were increased as the temperature was increased (in the selected temperature range). The maximum flexural strength and modulus were related to the 240 °C, which were 155 MPa and 8.6 GPa, respectively. However, it was reported that the surface accuracy of the manufactured specimens, due to the overflow of molten PLA, was lost. So, as the optimizing the lower temperature, which was 230 $\mathring{C}$ was reported, according to have high flexural strength and modulus, and the reasonable surface accuracy. Normally, the final printed parts with a smoother surface and also without deflection and distortion are considered as desired printed parts in viewpoints of reasonable surface and dimension accuracy.

More details from the effect of temperature on the mechanical properties have been achieved by studying the multiple interfaces, which were the interfaces between fiber and matrix. Deposited adjacent lines and layers.

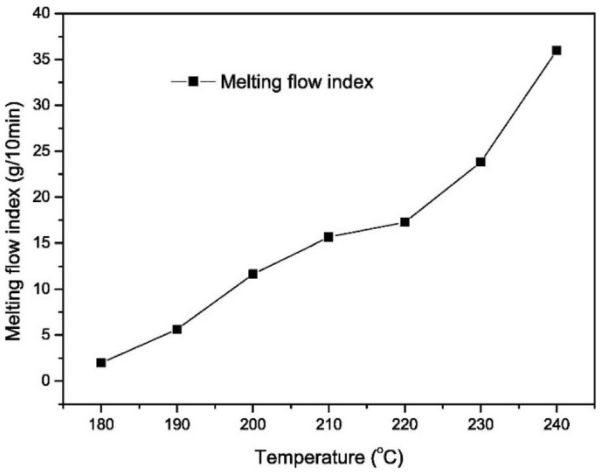


**Fig. 18** Melting flow index of PLA with temperature from 180 °C to 240 °C [39]

It was observed that the delamination was prepared between layers, because of inadequate bonding in the lower temperature of liquefier (180 °C) according to Fig. 20(a). But, by increasing the temperature up to 240 °C, no interface between the layer were not observed, because of increase of flowability of melt plastics by temperature (Fig. 20(d)). As an observation of the interface between the matrix and fibers, the impregnation of the matrix into the fiber bundle wasn't occurred in the lower temperature (180 °C) according

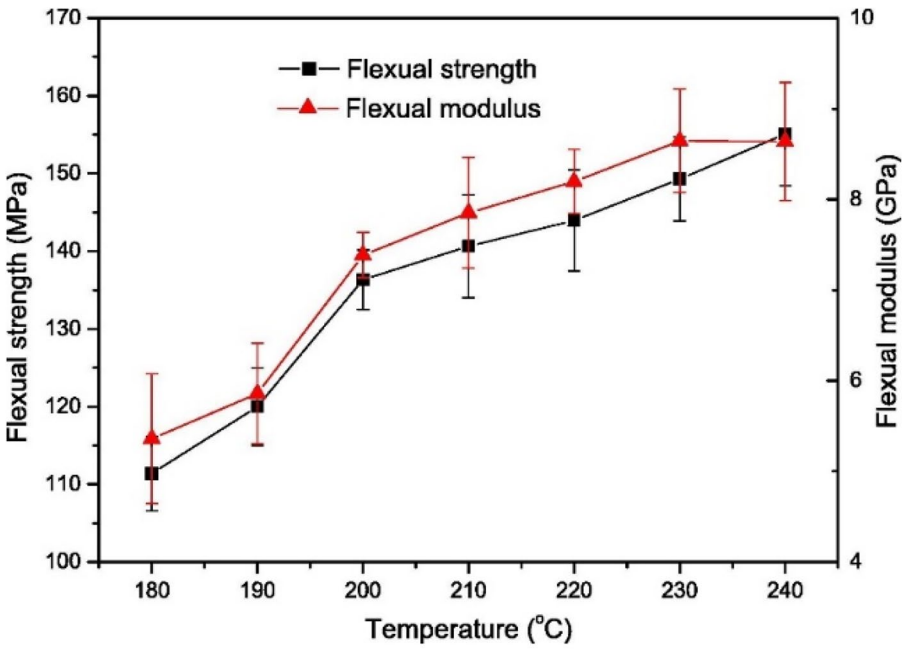


**Fig. 19** Effect of the liquefier temperature on the flexural strength and modulus of 3D printed continuous carbon fiber reinforced PLA composites [39]

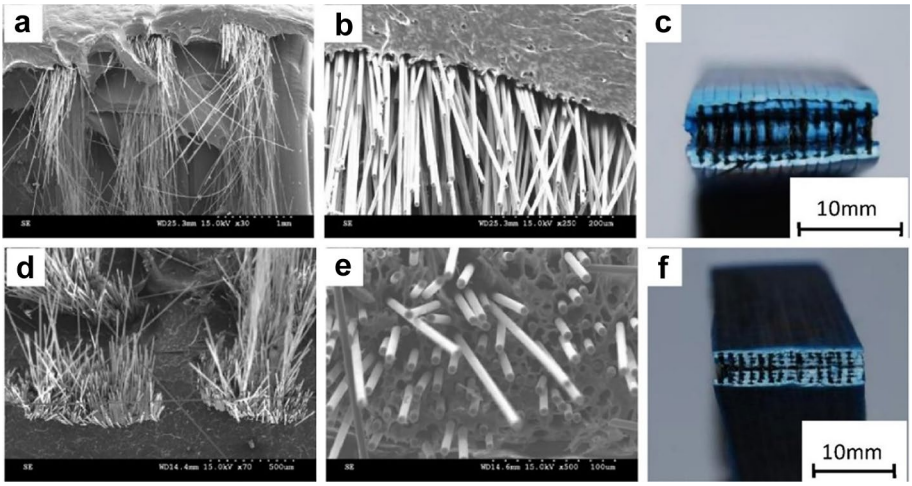


**Fig. 20** Microstructures of the obtained fractured cross-section from the applied flexural test on the carbon fiber PLA composites with liquefier temperature of 180°C (a, b, c) and 240°C (**d**, **e**, **f**), respectively: (**a**) and (**d**) overall cross-section, (**b**) and (**e**) interface, (**c**) and (**f**) fracture pattern [39]

to the Fig. 20(b), but by increasing the temperature up to 240 °C, the impregnation of PLA into the carbon fiber bundle was achieved (Fig. 20(e)). As the reason, by increasing the temperature, the melt flow index of the matrix was increased. It was observed that the matrix was broken first and could not transfer the applied load to the reinforcement fibers at lower temperatures. The fibers were pulled out (Fig. 20(c)). However, by increasing the temperature, the pattern of the fracture was changed, in which the fiber bundle breakage was observed (Fig. 20(f)). Therefore, that is why the flexural strength was increased by temperature increase.

As the study on the layer thickness parameter, the thickness of 0.3 mm to 0.8 mm was selected [39]. The flexural strength was decreased by an increase in thickness value, according to Fig. 21.

In fact, the tight space for the just deposited melt materials and increasing of the contact pressure between the nozzle and surrounding deposited lines were prepared, by decrease of the layer thickness. As more detail, the microscopic observations were applied. In the case of the smaller thickness (0.5 mm), it was observed that the homogenous bonding between the layers without obvious delamination in the interfaces was achieved (Fig. 21(a)), also the carbon fiber bundles were impregnated with matrix (Fig. 21(b)), and the load was transferred from PLA to carbon fibers, as was revealed during the fractography. However, in the case of the larger layer thickness (0.7 mm), the weaker bonding (Fig. 21(d)), inadequate impregnation (Fig. 21(e)), and fiber pull-out and shear delamination were observed (Fig. 21(f)).

The hatch spacing was studied from 0.4 mm to 1.8 mm. It was understood that as the hatch spacing was decreased from 1.8 mm to 0.4 mm, the average flexural strength and modulus were improved, simultaneously, from 130 to 335 MPa and 6.26 GPa to 30 GPa, respectively (Fig. 22).

As microscopic observations, by decreasing the hatch spacing from 1.6 mm to 0.6 mm, the impregnation of the matrix into the carbon fiber bundle was improved, according to Fig. 23.

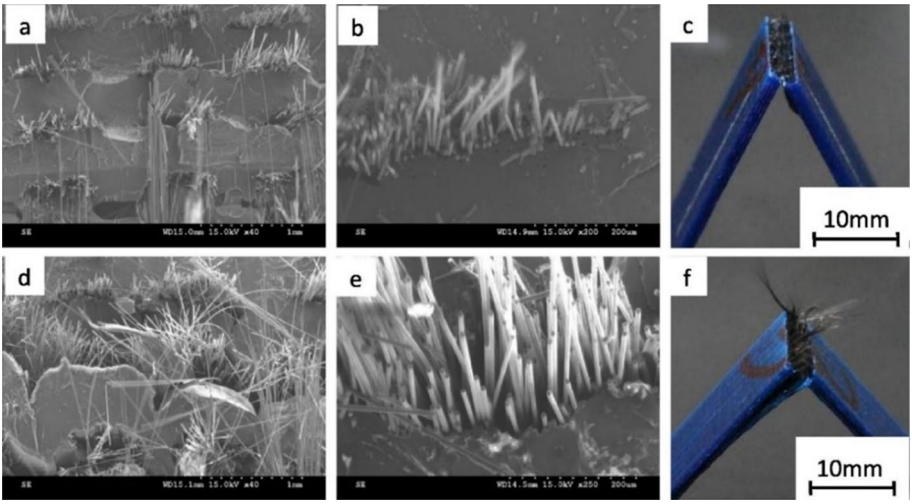


**Fig. 21** Microstructures of the obtained fractured cross-section from the applied flexural test on the carbon fiber PLA composites with a layer thickness of 0.5 mm (**a**, **b**, **c**) and 0.7 mm (**d**, **e**, **f**), respectively: (**a**) and (**d**) overall cross-section, (**b**) and (**e**) interface, (**c**) and (**f**) fracture pattern [39]

The feed rate of the filament (E) and the printing speed was studied, too. The feed rate of the filament affected the pressure and extrusion speed of molten material in the printing head and nozzle. According to Fig. 24, by increasing the feed rate from 60 mm/min

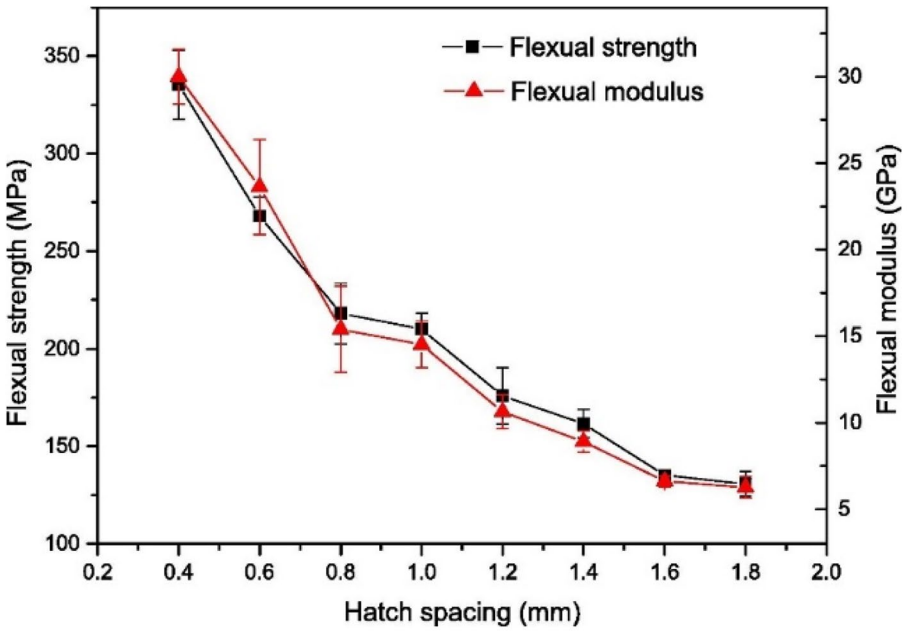


**Fig. 22** Influence of hatch spacing on the flexural strength and modulus of the 3D printed carbon fiber PLA composites [39]

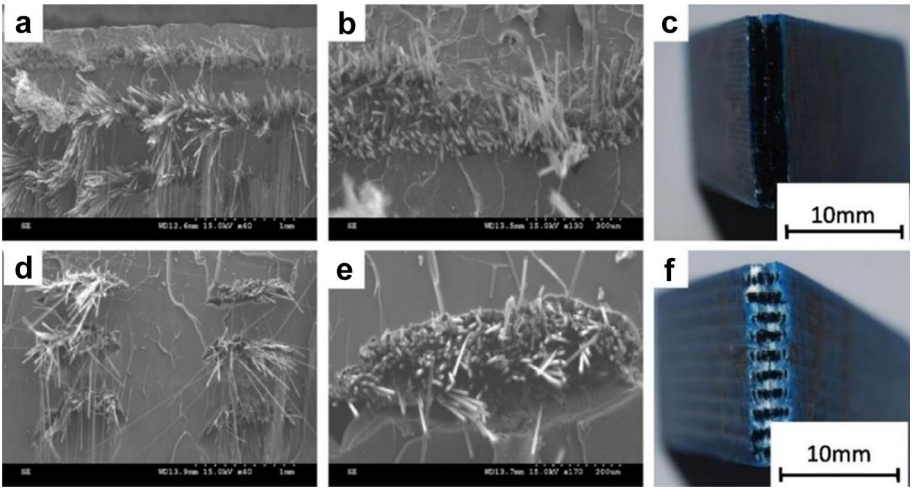


**Fig. 23** Microstructures of the obtained fractured cross-section from the applied flexural test on the carbon fiber reinforced PLA composites with hatch spacing of 0.6 mm (**a**, **b**, **c**) and 1.6 mm (**d**, **e**, **f**), respectively: (**a**) and (**d**) overall cross-section, (**b**) and (**e**) interface, (**c**) and (**f**) fracture pattern [39]

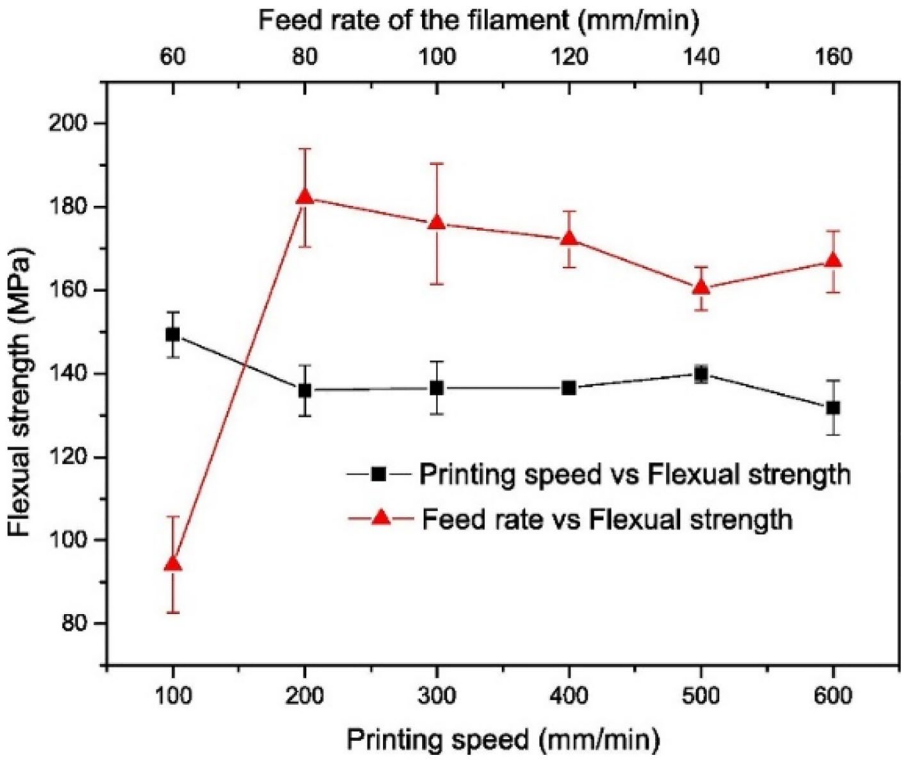


**Fig. 24** Influence of feed rate of the filament and printing speed on the flexural strength of the 3D printed carbon fiber PLA composites [39]

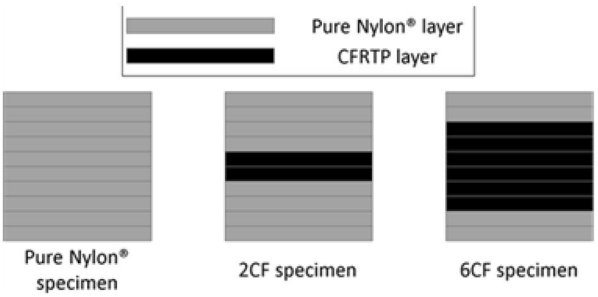


**Fig. 25** Schematic drawing of the three types of samples created by the Mark One® From left to right: 100% Nylon® specimen, 2CF specimen, 6CF specimen [42]

to 80 mm/min, the flexural strength of the PLA composite was increased. But the flexural strength of the composite wasn't improved anymore, by furthermore increasing the feed rate. The reason for this phenomenon could be the short impregnation period. The printing speed was found as an insignificant impact on the flexural strength, according to Fig. 24. As its reason, it was stated that the two contradictory factors which were the impregnation period, then pressure, and overall fiber contents, were influenced the flexural strength versus the printing speed.

Frank van der Klift et al. [42], studied the printed carbon fiber reinforced thermoplastic (CFRT) composite, fabricated by Mark One® printer. Three kinds of tensile test specimens were printed according to Fig. 25, with the same thickness and the quantity of the layers (10 layers). In fact, the first kind of the printed specimens were made of 100% Nylon (10 layers). The second type of the prepared samples (6CF) consisted of two layers of Nylon, six middle layers of carbon fiber reinforced thermoplastic, and two layers of Nylon, again. The third kind of printed specimens (2CF) was composed of four layers of Nylon, then two middle carbon fiber reinforced thermoplastic composite, and the four layers of Nylon.

The 6CF specimens showed more tensile strength in comparison with other stated specimens. The tensile strength of the 2CF specimens was about one-third of the prepared 6CF. The cross-section of the 2CF and 6CF specimens were exposed to micro-observation, according to Fig. 26. The observed void areas in 6CF were more in comparison with

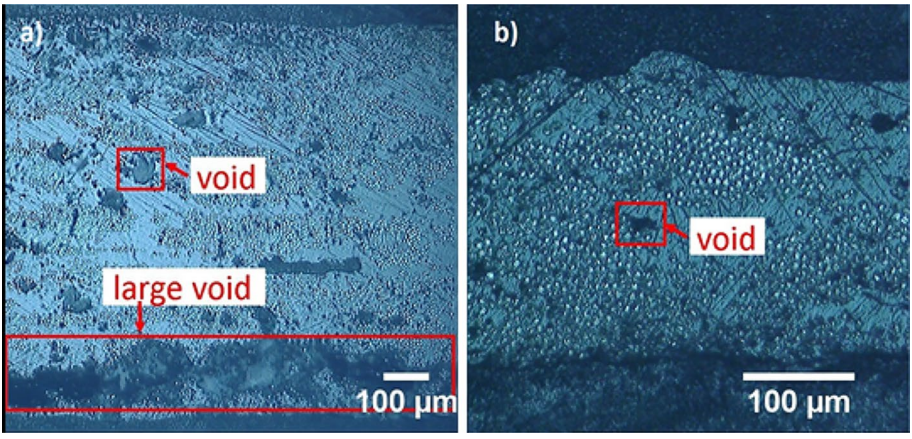


**Fig. 26** Cross-sections of the carbon fiber (2 and 6 layers) reinforced Nylon specimens. (**a**): It shows a cross-section of the 6CF specimen. (**b**): It shows the cross-section of a 2CF specimen. As can be seen, there is a lot more void area visible in (**a**) than in (**b**) [42]

2CF specimens. In addition, it has been reported that the 2CF specimens were close to the rule of mixing for the composite specimens that were made by the conventional methods, against the 6CF specimens were not close. The existence of more void areas in 6CF has been stated as the reason for this matter.

Kuldeep Agarwal et al. [43], studied on comparison of composite filament fabrication (CFF) which was Nylon-fiberglass reinforced polymer, and conventional composite processes, which was Epoxy-fiberglass, made by wet lay-up and vacuum bagging. System 1000 Epoxy resin with stated viscosity of 850 cps at 77 °F and Saertex 955 g/m2 stitched unidirectional fiberglass have been utilized for matrix and reinforcement, respectively. The process parameters' effect on the mechanical properties of the printed composite were studied. The tensile test and fatigue test were conducted to evaluate the mechanical properties. The dimensions of the tested specimens were 250 mm long, 25 mm wide, and 2.5 mm thick. The standards of ASTM D3039 and ASTM D3479,28 have been utilized for tensile and fatigue tests, respectively. The tension-tension fatigue test at the frequency of 5 Hz was applied. The applied parameters have been related to fiber volume fraction and fiber-layering technique. In the concentric infill pattern related to reinforcements, fiber rings were printed around the perimeter of the specimen, from the outer to the inner section of the specimen. In addition, in the isotropic infill pattern, fiber reinforcement is printed linearly and unidirectionally in a considered direction in a horizontal plane.

According to the mean stress–strain curves, related to the tensile test, (Fig. 27), the prepared specimens with a higher volume fraction of fiber, showed higher strength. The printed composite was stronger than the prepared composite by wet lay-up and vacuum bagging. The isotropic fill related to 0° orientation had a higher strength. Also, the 45° and 90° orientation had lower strength, in comparison with the 0° ones. In the comparison to the used conventional method, it was reported that the manufactured specimens by wet lay-up had about 30–40% lower strength in comparison with manufactured specimens by vacuum bagging. Also, the better adhesion between the layers, which probably caused the delamination between the layers of the prepared composite, by wet lay-up, was the main failure mechanism.

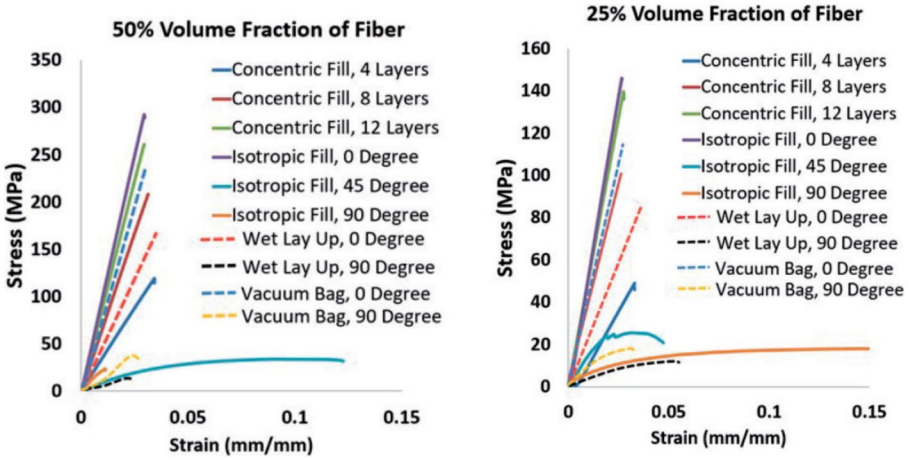


**Fig. 27** Stress–strain curves after tensile test of 3D printed Nylon-fiberglass composites, compared with Epoxy-fiberglass composites manufactured by conventional composite processes for range of fiber orientations [43]

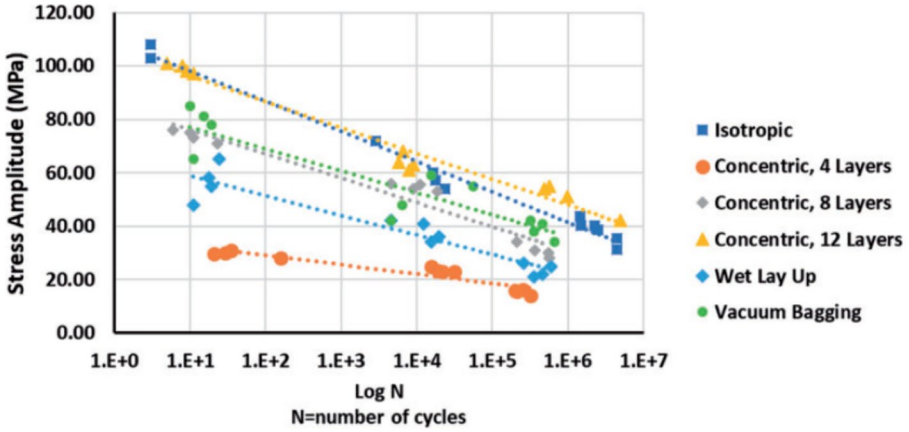


**Fig. 28** Fatigue lifetime for 25% volume fraction related to 3D printed Nylon-fiberglass composites, compared with Epoxy-fiberglass composites manufactured by conventional composite processes, 0° orientation [43]

According to Figs. 28 and 29, the prepared 50% volume fraction composites had better fatigue performance in comparison with the prepared 25% volume fraction, according to the tension-tension fatigue results at the frequency of 5 Hz (Figs. 27 and 28). The printed isotropic longitudinal composite (0°) showed the highest fatigue property followed by the printed concentric, 12-layers specimens. Also, the vacuum bagging, as a conventional process, resulted in parts that had a fatigue performance just near to the concentric composite, also about 70–80% of the printed isotropic composite.

Oztan et al. [44], studied the microstructures related to the various three-dimensional-printed continuous fiber composites and their connection to the mechanical test results, which the tensile test was considered. The printed prepared samples were unidirectional carbon fibers in nylon matrix, unidirectional Kevlar fibers in nylon matrix, and Kevlar fibers in nylon matrix in the directions of $\pm 45°$. Also, the unreinforced nylon specimens

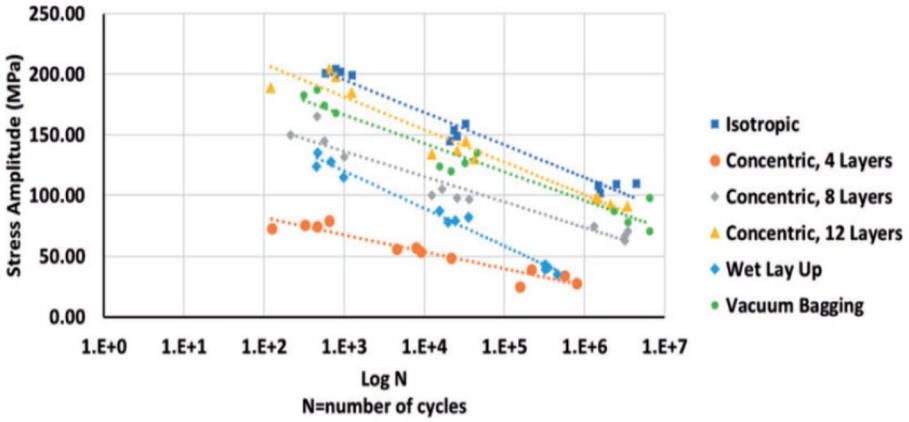


**Fig. 29** Fatigue lifetime for 50% volume fraction, 0° orientation [43]

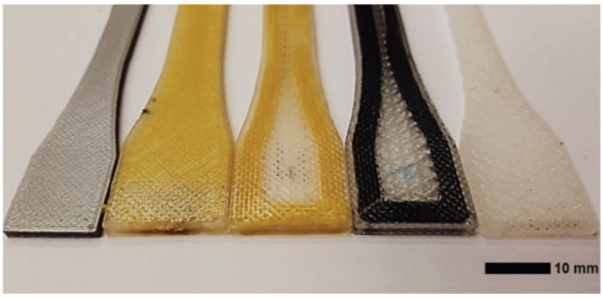


**Fig. 30** 3D-printed samples were used in the research. Left to right: PLA sample produced using Ultimaker 2 printer, ±45° Kevlar fiber, unidirectional Kevlar fiber, unidirectional carbon fiber, and unreinforced nylon matrix [44]

with 100% fill density were printed by Mark One printer. The PLA specimens were printed in 100% fill density condition, by Ultimaker2 printer (Fig. 30).

The comparison between the manufactured polymer specimens by 3D printing and traditional methods (in which the PLA and nylon filament samples from the supply coil of the printer were used), was made, too. The related tensile test results of the unidirectional and the printed PLA and nylon were according to Fig. 31. According to the tensile test results, the tensile strengths of the printed polymers were lower than those, which were traditionally fabricated. This distance between the tensile strengths, were more obvious, in the case of the nylon samples. In fact, the related ultimate strength of the printed nylon was reported as half of the nylon's samples, which were traditionally fabricated. Also, the start of the stiffness loss has happened in the printed specimens, firstly in comparison with the traditionally fabricated ones. It was reported that the maximum tensile strain values were independent of the manufacturing methods, against the ultimate stress.

Then, the microscopic observations were applied according to Fig. 32. Figure 32(a) is related to the cross-hatched pattern. The imperfect fusion of the layers (between the layers) is visible clearly. Also, a common defect of the printed material, which is the rectangular gap, was observed in Fig. 32(b). Figure 32(c) is related to the insufficient material interdiffusion between the printed lines, which causes the surface roughness on the upper print face. Figure 32(d) is reported as the related SEM photo to the observed porosities in PLA samples, which caused the mechanical properties reduction.

Therefore, according to the tensile test results of the printed reinforced composites (Fig. 33), it was reported that all tensile tested specimens had a linear-elastic behavior. The comparison between the matrix and the fiber types, also their related orientation, is

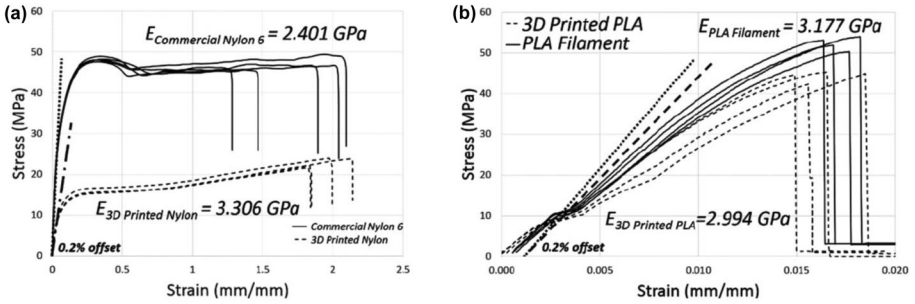


**Fig. 31** Stress–strain curves of the 3D-printed and traditionally fabricated polymers (**a**) Nylon specimens and (**b**) PLA specimens [44]

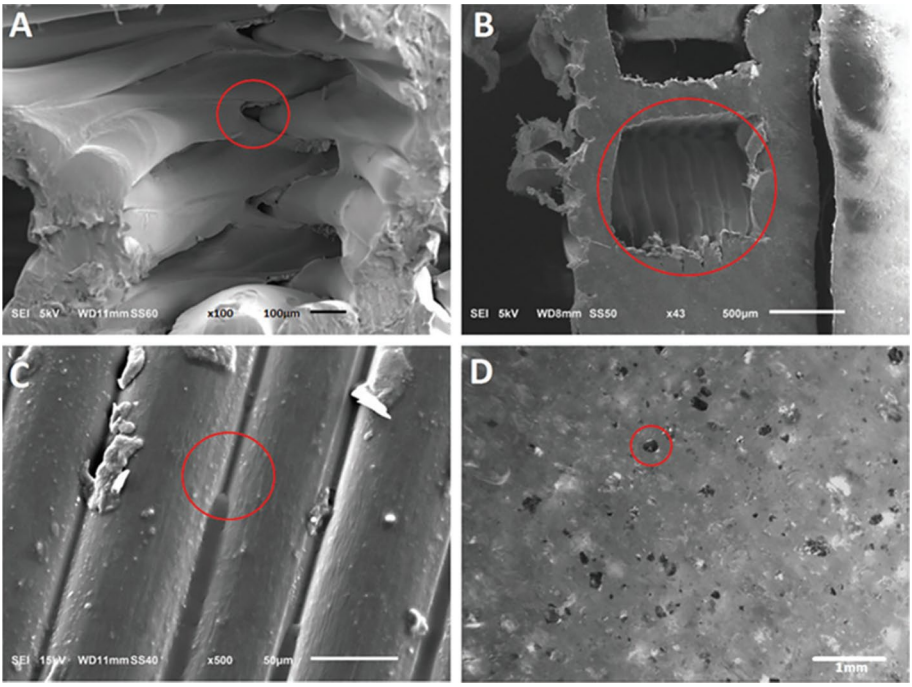


**Fig. 32** Microstructural defects in 3D-printed, unreinforced polymer specimens. (**a**) Crosshatch voids in nylon sample, (**b**) fiber tow gaps in nylon sample, (**c**) surface roughness in nylon sample, and (**d**) micropores at the surface of PLA sample [44]

clear according to Fig. 32. The printed carbon fiber reinforced composites had the highest tensile strength and the lowest failure strain, in comparison with the Kevlar fiber-reinforced composites. The fabricated Kevlar-reinforced composites, in the orientation of $\pm 45°$, had lower tensile strength in comparison with the unidirectional ones. It was reported that the strength of the unreinforced nylon samples was increased by a factor of 2–11, depending on the specimen direction.

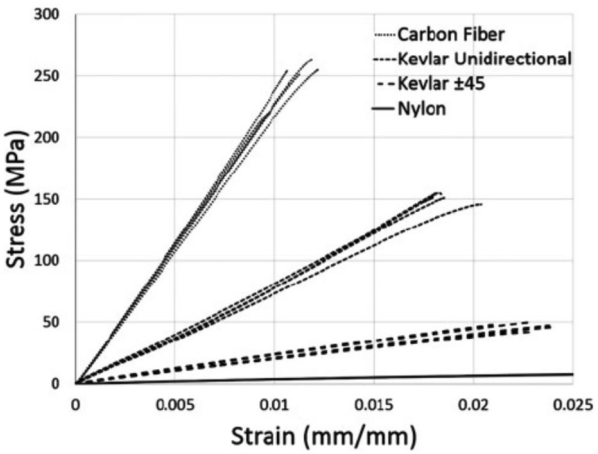


**Fig. 33** Stress–strain curves of the 3D-printed composites (unidirectional carbon fibers in nylon matrix, unidirectional Kevlar fibers in nylon matrix, $\pm 45°$-oriented Kevlar fibers in nylon matrix, also the unreinforced nylon specimens with 100% fill density, according to Fig. 29) [44]

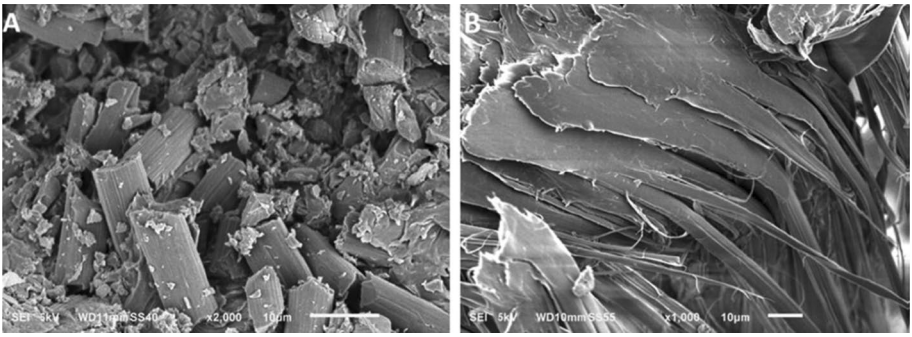


**Fig. 34** SEM images of fractured fibers, (**a**) carbon fibers showing brittle damage morphology, and (**b**) Kevlar fibers showing significant elongation and distortion, after tensile tests [44]

According to the related micro-observation (Fig. 34), the rupture of the carbon fibers was brittle; also there was no distortion or elongation of the broken ends. However, the fracture of the Kevlar fibers was ductile and the related elongation and distortion in the failure section were reported.

Dong et al. [45], studied on the continuous Kevlar fiber reinforced nylon thermoplastic, manufactured by Mark One printer as FFF process. Four parameters were considered to study to understand the mechanical properties development, by use of the continuous Kevlar fibers as reinforcement into 3D printer reinforced nylon composites. These four parameters were as below:

1) Effect of fiber orientation
2) Effect of the layer position
3) Effect of volume fraction
4) Effect of the infill orientation

In addition, the details of the samples were as Table 5.

As the effect of the fiber orientation, samples 8 and 9 were studied. Sample 8 was consisting of 5 layers of 0°-Kevlar fibers and 5 layers of 90°-Kevlar fibers. Also, sample 9 was

**Table 5** The design parameters of continuous Kevlar fiber reinforced composites (KFRCs) [45]

| Sample No | Total Layers | Layers of fibers | Direction of fibers | Position of fiber layers |
|---|---|---|---|---|
| 1 | 20 | 10 | 0 | 6–15 |
| 2 | 20 | 10 | 90 | 6–15 |
| 3 | 20 | 10 | 0 | 2–6, 15–19 |
| 4 | 20 | 10 | 90 | 2–6, 15–19 |
| 5 | 20 | 0 | - | - |
| 6 | 20 | 18 | 0 | - |
| 7 | 20 | 18 | 90 | - |
| 8 | 20 | 10 | 0°-5, 90°-5 | 6–15 |
| 9 | 20 | 10 | 45°-5, -45°-5 | 6–15 |
| 10 | Same as No.1 but with 0°- and 90°-degree Nylon | | | |

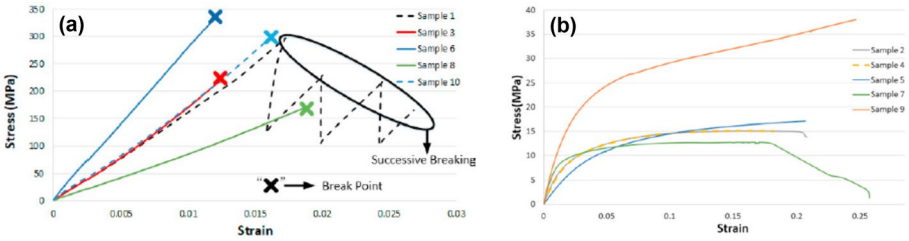


**Fig. 35** Stress–strain curve and breaking points of 3D printed Kevlar fiber reinforced PLA composite with layups shown in Table 5 (**a**) samples 1, 3, 6, 8, 10 and (**b**) 2, 4, 5, 7, and 9 [45]

consisting of 5 layers of 45° fibers and -45° fibers. It was stated that the continuous Kevlar fiber showed high elastic modulus in the longitudinal direction. The Young's modulus and tensile strength of the continuous KFRs in this research were higher than the printed short fiber-reinforced composites, reported by [46]. As the effect of the layer position, it was concluded that the fiber position does not have influence the related tensile modulus of the fabricated continuous KFRCs, by FFF. Also, it was understood that the related tensile stress of sample 3 was lower than sample 1, at the break.

As the effect of volume fraction, it was stated that the higher volume fraction of the used Kevlar fibers, could improve related tensile stress and elastic modulus to the break. But the condition of the fiber and nylon matrix may be causing the lower ultimate strength and elastic modulus of the continuous Kevlar fiber-reinforced composites than the predicted value from the rule of mixtures. As the effect of the infill orientation, the related infill angles of Nylon in the printed composite samples were $\pm 45°$ by default, except sample 10. In fact, sample 10 was printed with 0° and 90° infill angles. The fiber direction in samples 1 and 10 was parallel to the tensile direction. It was stated that the effect of the infill angle of Nylon could be neglected, because it was much lower than the Kevlar fiber, according to the related stress–strain curves of sample 1 and 10. Also, this effect was studied by samples 8 and 9, too. The related stress–strain curves are as Fig. 35.

The failure mode of the tested samples was debonded on the Kevlar fibers orientation. In the case of the unidirectional specimens, in which the Kevlar fiber was in the same direction of the applied stress, the breakage of the unidirectional fibers was reported as the reason for the failure (Fig. 36(c)). Also, in the case of the 90° fibers (perpendicular to the applied tension stress), the failure between two fiber filaments was

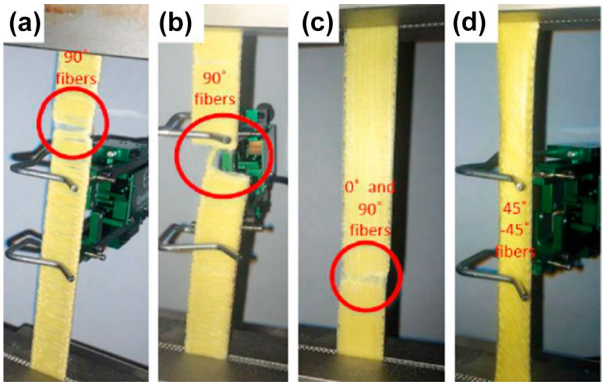


**Fig. 36** (**a**) failure of sample 4, (**b**) failure of sample 7, (**c**) failure of sample 8, and (**d**) shear deformation of fibers in sample 9 [45]

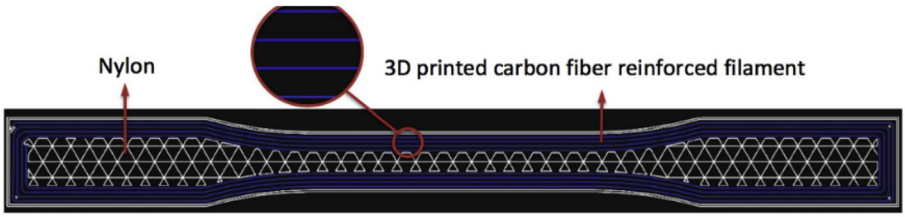


**Fig. 37** The related 2D internal layer structure of a manufactured continuous carbon fiber reinforced Nylon by 3D printing [47]

reported (Fig. 36(a) and (b)). In case of the failure, related to $\pm 45°$ specimens, it was stated that the fibers did not break during the tensile test. The debonding between the Kevlar and nylon layers was stated as the reason for the $\pm 45°$ printed specimens. Generally, the difference between the Poisson's ratio of nylon and fiber layers was stated as the reason for the fiber-nylon layers debonding.

Nekoda van de Werken et al. [47] investigated the mechanical properties of the manufactured continuous carbon fiber reinforced Nylon by 3D printing. The specimens were printed utilizing a Markforged commercial printer (Fig. 37).

The microstructure of the 3D printed continuous carbon fiber reinforced Nylon samples were characterized. The printed specimens were cut for cross-sectional microscopic observations. The microscopic observations showed that a huge number of voids were existed in the manufactured specimens by FFF. The existence of the voids was introduced as the reason for the failure of the samples at the lower stresses in comparison with the theoretically predicted stresses (Fig. 38).

According to the tensile tested specimens, the various failure modes such as delamination, inter-filament failure, and fiber failure were observed, like the prepared composite parts by conventional methods. According to the fiber pullout phenomenon observations, the weakness of the related interfacial strength between the matrix and reinforcement was shown (Fig. 39).

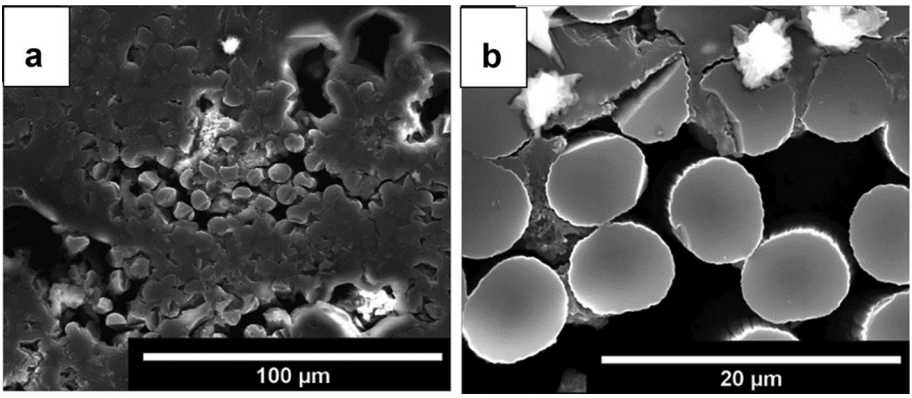


**Fig. 38** The cross-sectional microstructure of the 3D printed carbon fiber reinforced Nylon specimens (**a**) the existence of the voids in the 3D printed composite, (**b**) the carbon fibers as for the reinforcement in the 3D printed carbon fiber reinforced Nylon composite [47]

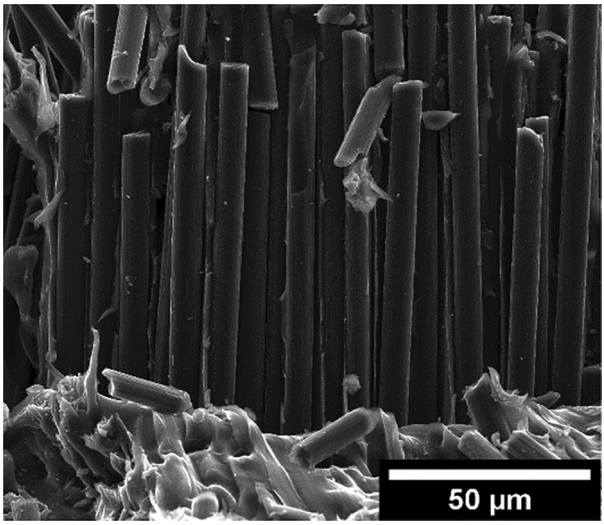


**Fig. 39** The fiber pullout phenomenon in the 3D printed carbon fiber reinforced Nylon composite [47]

It was stated that the approached strength of the manufactured specimens by 3D printing strictly depends on the part geometry and infill pattern. In fact, the interfaces between the non-reinforced and reinforced sections and regions and the fiber curvatures caused the multi-axial stress states, stress concentrations, and pre-mature failure in the printed parts.

Ali N. Sarvestani et al. [48] studied the effects of volume fraction and fiber orientation on mechanical properties of the manufactured carbon fiber reinforced polymer composites (CFRP) by FFF. Post fracture microscopy observations (Fig. 40) exhibited the fiber pullout phenomenon. The fiber pullout demonstrated that the interfacial strength between the fiber and polymer matrix was relatively low.

Different tensile test sample geometries related to carbon fiber reinforced Nylon composite, which caused different fiber volume fractions in the gauge section, were taken

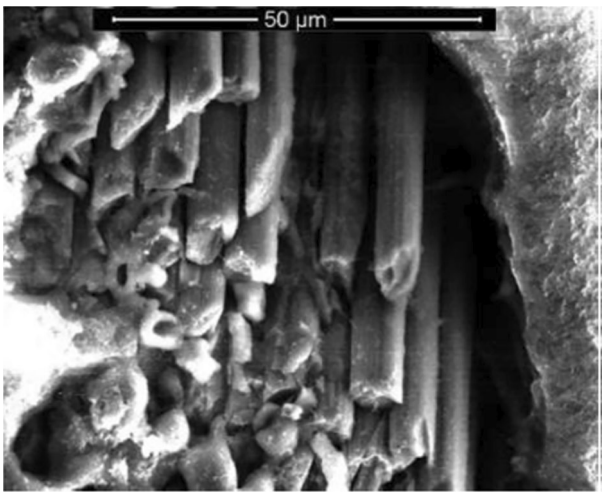


**Fig. 40** Post fracture microscopy observation 3D printed carbon fiber reinforced Nylon composite samples showing fiber pullout [48]

into account. The stated samples were printed by consideration of the different configurations for fiber orientation. Any of the samples weren't broken in the gauge section and none of the samples failed just because of the fiber failure phenomenon. Other modes of damages such as fiber pull, matrix cracking, and delamination were reported (Table 6).

Yolnan Chen et al. [49] studied the effect of the orientation of the used continuous reinforcement on the tensile strength of the manufactured part by FFF. The considered orientations were "concentric" and "isotropic" infill. According to concentric layout, the reinforcement rings printed along the boundary walls of the part, but according to the isotropic fill the reinforcement located at the desired orientation in the one complete layer (Fig. 41).

PLA, ABS, nylon as for polymers, also Carbon fiber, glass fiber, and Kevlar fiber were used as reinforcements. In the case of composite fabrication, the nylon used as matrix and the stated fiber reinforcement materials were applied by Markforged printer.

Firstly, the carbon fibers were used for reinforcing the all below stated geometries and infills via FFF method (Table 7). Then the best fiber orientations, which showed the highest yield stress were selected, and tested with Kevlar fibers and glass fibers.

As for concentric infill type, Fig. 42 exhibits the related stress–strain graph of the concentric fill reinforced nylon. The strongest specimen was reinforced by five concentric fiber rings (the highest-fiber volumetric fraction), which had a fracture stress level of 250 MPa. In addition, the reinforced specimens by two concentric fiber rings were the weakest ones.

Figure 43 is related to tensile test results of isotropic fill reinforced nylon. According to the below-obtained results, the reinforced specimens by isotropic infill with two concentric rings of the reinforcement exhibited the highest strength. The volumetric fraction of the reinforcement was reported as almost constant for all of the printed specimens.

**Table 6** Tensile test results and prevalent damage modes of the 3D printed carbon fiber reinforced Nylon composite samples, by Mark Two, Markforged [48]

| Sample Description | Fiber volume fraction in the gauge section | Modulus of Elasticity (GPa) | Failure Strength (MPa) | Prevalent Damage Mode (failure region) |
|---|---|---|---|---|
| ASTM D638-14 Type 1  | 5 | 7.2 | 94.7 | Matrix failure (grip region) |
| | 12 | 17.5 | 258.1 | Matrix failure (grip region) |
| | 14 | 21.3 | 265.8 | Matrix failure (grip region) |
| | 28 | 55.7 | 270.4 | Delamination (grip region) |
| ASTM D638-14 Type 4 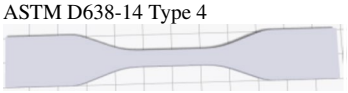 | 24 | 46.1 | 171.9 | Matrix failure (grip region) |
| ASTM D3039/D3039M – 14 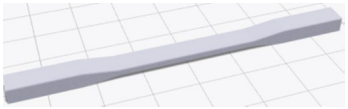 | 30 | 52.4 | 580.0 | Fiber Failure + Delamination (gauge region) |

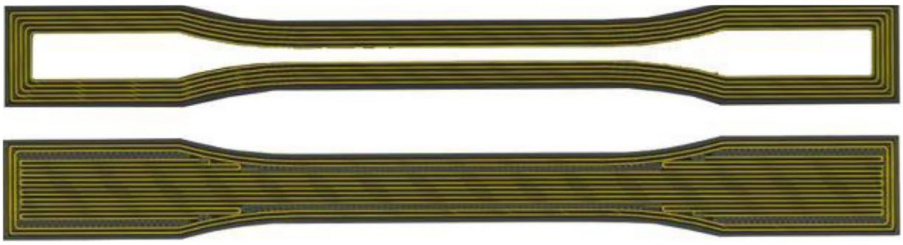

**Fig. 41** Cross-section view of concentric (top) and isotropic (bottom) infills [49]

The two aforementioned strongest fiber orientations were considered, and the specimens were printed with KV and FG, too. The reinforced specimens with CF showed the highest yield strength, while the obtained deformation resistance to fracture was lower in comparison with the reinforced sample by FG and KV. The comparison between the different types of reinforcement materials is prepared in Fig. 44.

Astrit Imeri et al. [50], studied the effect of infill type and the fiber pattern on tension-tension fatigue characteristics under load ratio of 0.1 of 3D printed polymer composite. Nylon was selected as the matrix of the composite and the specimens were produced by Markforged Mark Two 3D Printer. The specimens were printed under "concentric" and "isotropic" infill patterns. The stated the existence of a correlation between the type of the used filler material and the selected infill pattern of the reinforcement printing. In fact, the carbon fiber exhibited a better fatigue resistance in comparison with other used reinforcements (glass fiber and Kevlar fiber). In the case of printing with the concentric pattern, the increase of the rings increased the fatigue life. As for the isotropic infill pattern, the fatigue behavior decreased by increasing the number of reinforcement rings.

Table 8 presents the summary of extracted mechanical data for continuous fiber systems loaded parallel to the printing direction. One can note from this table the effect of fiber percentage on the tensile strength and tensile modulus. By increasing the reinforcement volume fraction the tensile properties were increased. Moreover, the reinforcement type has a significant effect on the mechanical properties.

**Table 7** Table of the printed tensile specimens [49]

| Polymer Material | Fiber Material | Fiber Fill Type | Rings | Infill Type | Infill % | Machine |
|---|---|---|---|---|---|---|
| Nylon | None | None | 0 | Rectangular | 75 | Markforged |
| Nylon | Carbon | Concentric | 2 | Rectangular | 75 | Markforged |
| Nylon | Carbon | Concentric | 4 | Rectangular | 75 | Markforged |
| Nylon | Carbon | Concentric | 5 | Rectangular | 75 | Markforged |
| Nylon | Carbon | Isotropic | 0 | Rectangular | 75 | Markforged |
| Nylon | Carbon | Isotropic | 2 | Rectangular | 75 | Markforged |
| Nylon | Carbon | Isotropic | 4 | Rectangular | 75 | Markforged |
| Nylon | Carbon | Isotropic | 5 | Rectangular | 75 | Markforged |

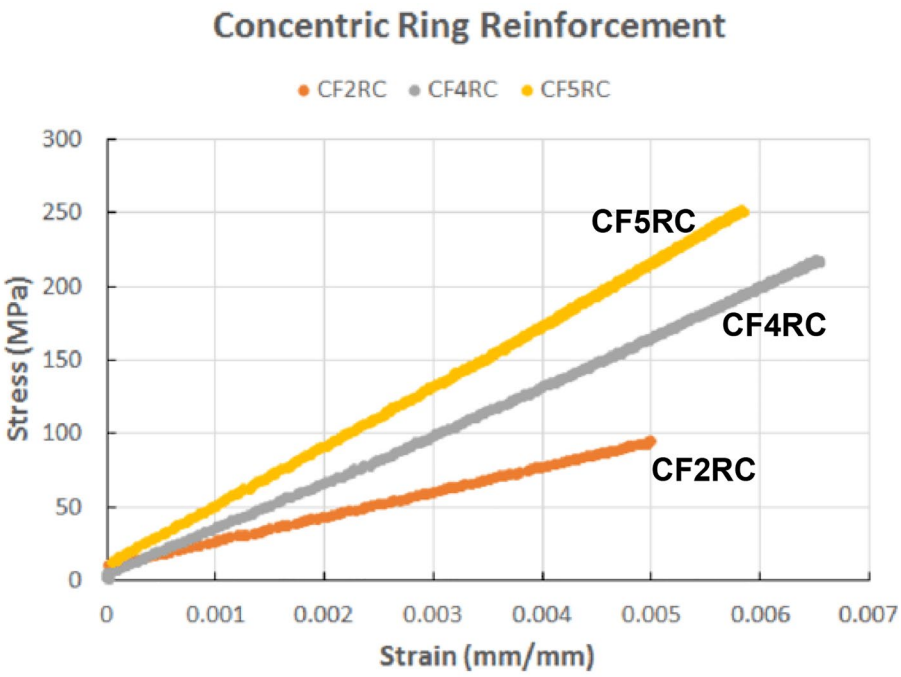


**Fig. 42** Stress–strain of the printed specimens with CF with concentric fiber rings. The selected concentric rings of Carbon Fiber were 2, 4, and 5 [49]

### 4.2.2 Short fiber-reinforced polymers

Weihong Zhong et al. [56], studied the fabrication of the reinforced ABS by short glass fibers as feedstock filament in the FFF process. As improving the properties of the ABS, short glass fiber as reinforcement was used. The strength of the short glass fiber reinforced ABS was increased, in comparison with the pure ABS. By use of the glass fiber reinforcement, the surface rigidity was developed, and the shrinkage was decreased. However, the handleability was decreased. In fact, the prepared composite feedstock wasn't possible to be made into a continuous wound on a conventional cylindrical shape drum, and this brittleness caused the impossibility of the use of the prepared composite feedstock in the FFF machine. By use of a small amount of compatibilizer and plasticizer, these properties of the prepared composite feedstock were improved.

Fuda Ning et al. [46], studied on fabrication and properties of the reinforced ABS by short carbon fiber feedstock. The effect of the carbon fiber content and length were studied on the mechanical properties of the fabricated samples. The used carbon fiber powders had two average lengths of 100 μm and 150 μm. The pellets of polymer (matrix) and carbon fiber powders (reinforcement) with different contents of 3 Wt%, 5 Wt%, 7.5 Wt%, 10 Wt%, and 15 Wt% were blended, then were extruded for manufacturing the feedstock filament for the FFF process, according to Fig. 45.

As the effect of the carbon fiber content on the tensile properties was surveyed (Fig. 46). As its effect on tensile strength, it was observed that with an increase of the used short carbon fiber content from 0 W Wt.t% to 5 Wt.%, tensile strength was increased, too. Then,

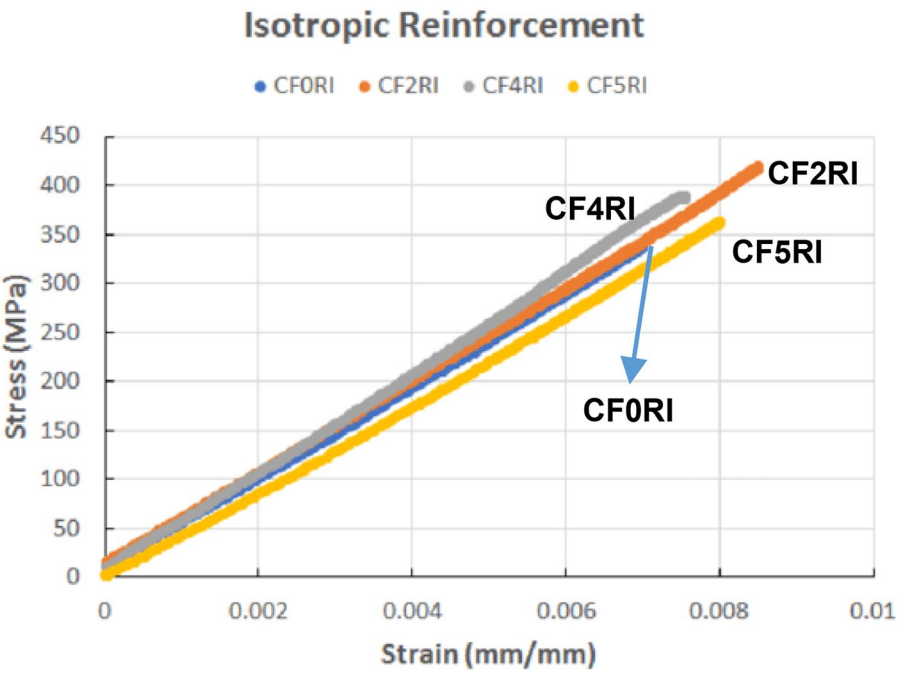


**Fig. 43** Stress–strain of the printed specimens with CF with isotropic infill of the carbon fiber. The selected Carbon Fiber infill were 0, 2, 4, and 5 rings isotropic infill [49]

with an increase of the carbon fiber content from 5 Wt.% to 10 Wt.% the tensile strength decreased. But the strength was increased with the increase of the carbon fiber content from 10 Wt.% to 15 Wt.%. As the effect of the carbon fiber content on the young's modulus, the increase of the young's modulus was observed by the increase of the reinforcement content from 0 Wt.% to 7.5 Wt.%. But the sudden decrease of the young's modulus was observed by the increase of the carbon fiber from 7.5 Wt.% to 10 Wt.%. Again, with the increase of the reinforcement content up to 15 Wt.%, the young's modulus was increased. The ductility decreased by increase the content of the carbon fibers from 0 Wt.% to 10 Wt.%. But the ductility increase was reported with the increase of the carbon content from 10 Wt.% to 15 Wt.%. The lowest ductility was related to unreinforced plastic specimens.

Also, the effect of the carbon fiber length on the tensile properties of the printed samples was studied (Fig. 47). It was observed that the tensile strength and young's modulus of the printed composite samples with 150 µm carbon fiber, were more than ones were printed using 100 µm carbon fiber. The composite samples with 100 µm carbon fiber, had more toughness and ductility in comparison with ones 150 µm as carbon fiber length. As microscopy observation, it was observed that in the specimens with 10 Wt.% carbon fiber content, the porosity was severest. This phenomenon was stated as the probable reason for the smallest values of the tensile strength, toughness, yield strength and ductility, in the printed samples by the use of the 10 Wt.% carbon fiber as the reinforcement.

Tenkinalp et al. [57], studied the effects of the two important parameters which were porosity and fiber orientation on the mechanical properties of the printed reinforced ABS, by short carbon fiber (0.2–0.4 mm). The related results of the printed samples also were

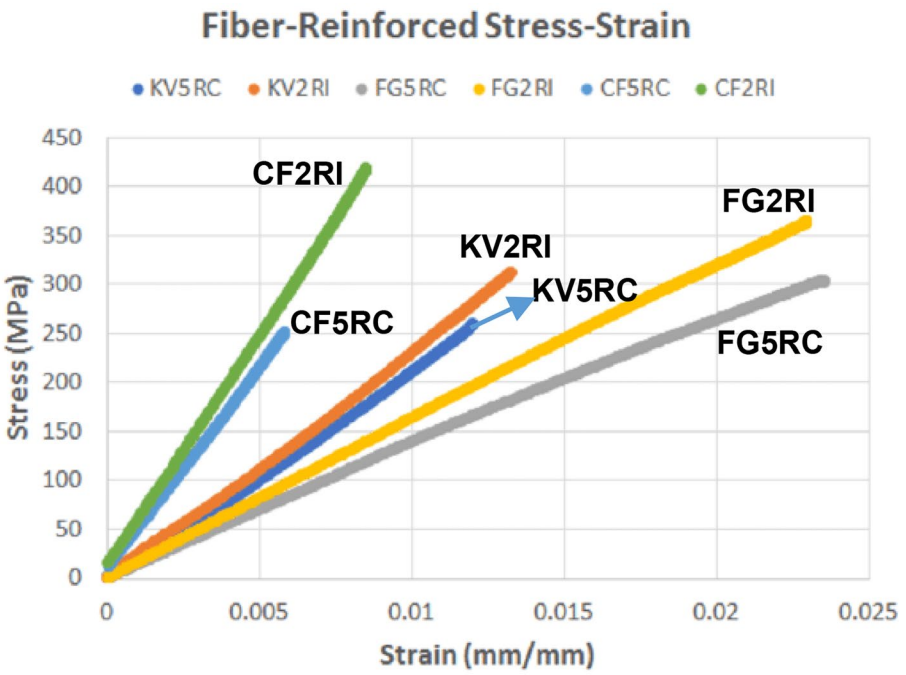


**Fig. 44** Tensile Stress–strain curves related to tensile specimens using the two best-obtained fiber orientations [49]

**Table 8** Summary of extracted mechanical data for continuous fiber (AF: Aramid Fibers, GF: Glass Fibers, and CF: Carbon Fibers) systems loaded parallel to the printing direction

| References | Materials | Tensile strength (MPa) | Tensile modulus (GPa) |
|---|---|---|---|
| Dickson et al. [51] | Nylon/CF 11vol.% | 198 | 8.46 |
| | Nylon/AF 8vol.% | 110 | 4.23 |
| | Nylon/GF 8vol.% | 156 | 3.29 |
| | Nylon/AF 10vol.% | 161 | 4.76 |
| | Nylon/GF 10vol.% | 212 | 4.91 |
| Van der Klift et al. [42] | Nylon/CF 6vol.% | 140 | 14 |
| | Nylon/CF 18vol.% | 464.4 | 35.7 |
| Yang et al. [52] | ABS/CF 10wt.% | 147 | 4.19 |
| Tian et al. [53] | PLA/CF 10wt.% | 256 | 20.6 |
| Li et al. [38] | PLA/CF 34vol.% | 91 | 23.8 |
| Melenka et al. [54] | Nylon/AF 4vol.% | 31 | 1.77 |
| | Nylon/AF 8vol.% | 60 | 6.92 |
| | Nylon/AF 10vol.% | 84 | 9 |
| Matsuzaki et al. [36] | PLA/CF 6.6vol% | 185.2 | 19.5 |
| | PLA/Jute fiber 6.1vol% | 57.1 | 5.11 |
| Bettini et al. [55] | PLA/AF 8.6 vol. % | 203 | 9.34 |

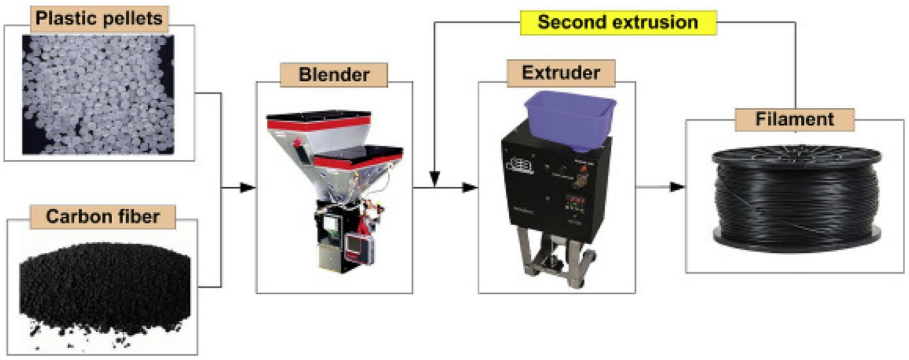


**Fig. 45** Manufacturing the feedstock filament for the FFF process [46]

compared with the prepared composite parts, by compression molding (CM). The printed samples had void formation which was due to the inappropriate adhesion and bonding between the polymer matrix and fiber reinforcement, according to the Fig. 48. As a comparison against the printed samples, there was almost no voids in the samples which were prepared by compression molding (CM). The printed samples were very high fiber oriented

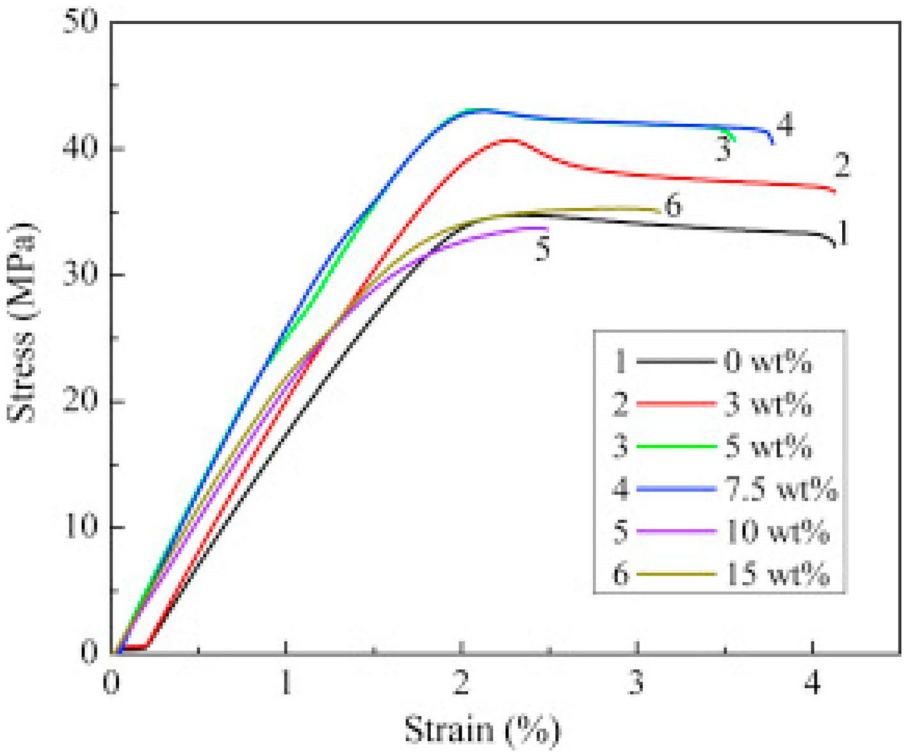


**Fig. 46** Typical tensile strain–stress curves for specimens with different carbon fiber contents (The carbon fiber length is 150 μm), related to carbon fiber reinforced ABS composite [46]

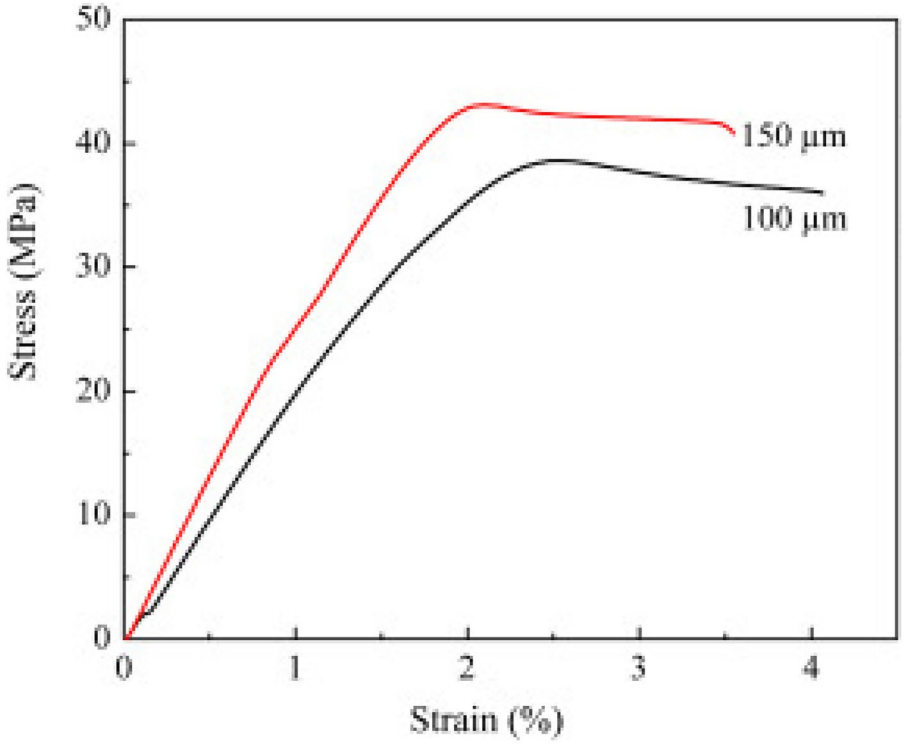


**Fig. 47** Effects of carbon fiber length (Carbon fiber content is 5 Wt.%), related to carbon fiber reinforced ABS composite [46]

but the prepared composite parts by CM were less oriented. As the tensile test results, the related results of the printed specimens were almost close to the prepared ones by compression molding (CM). In fact, two main parameters completed and affected strength, which were the orientation of the fibers and existence the negative porosity. In the case of the printed samples, the fibers were in direction of the applied load and could overcome the negative effect of the porosity existence.

In addition, it was reported that the tensile strength of the printed neat-ABS samples was higher than the neat-ABS prepared by CM. As a result, it was stated that the FFF method increased the molecular orientation of the polymer chains, which increased the tensile strength in the FFF process. Also, as the content of the fiber was increased, the voids between the beads decreased, but the void content inside the bead, increased.

Lonnie J. love et al. [58], studied the reinforced ABS by short carbon fiber composite parts. They showed that the use of carbon fiber (CF) with polymer (matrix) as a feedstock of AM process could increase the stiffness and strength of the final printed parts. They could demonstrate that the use of CF, can decrease the coefficient of thermal expansion (CTE) and increase the thermal conductivity, which greatly caused the reduction of the distortion of the final printed parts. In fact, by the increase of the thermal gradients were reduced through the final printed parts. Also, by reducing the CTE, the strain of the material during the cooling from the deposition temperature to ambient conditions decreased.

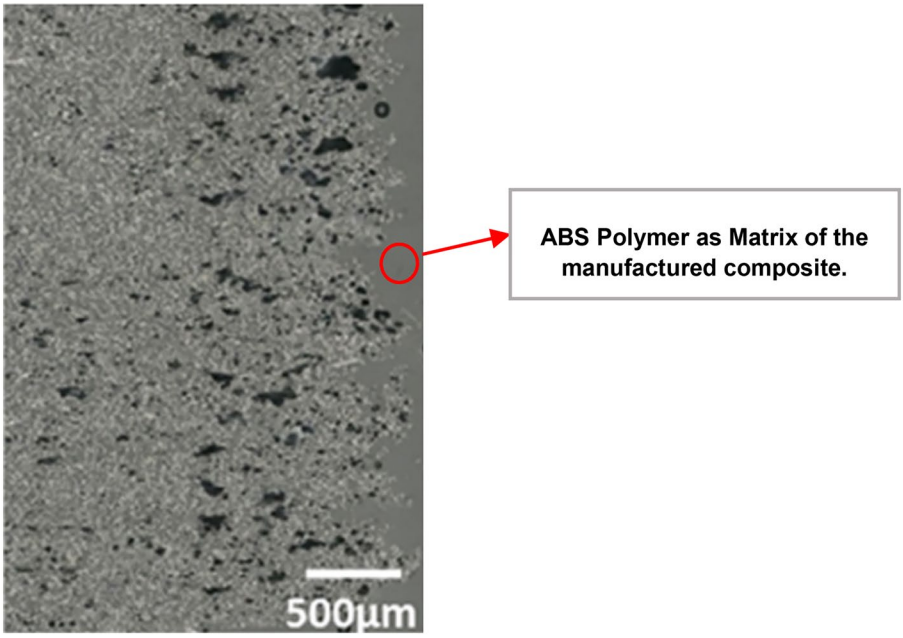


**Fig. 48** Micrograph of the polished surface of the printed ABS/30 Wt.% carbon fiber composite [57]

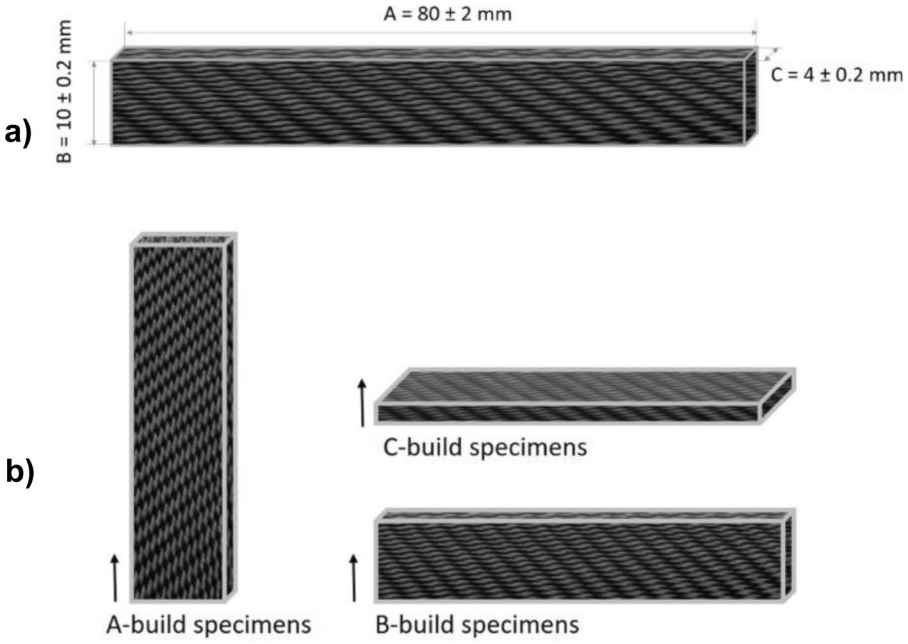


**Fig. 49** (**a**) The geometry of the printed specimens according to ISO 179, (**b**) Naming of the specimens built along different axes [59]

So, the impacts of these two important factors could reduce the distortion of the parts during additive manufacturing.

Yasa et al. [59], studied the impact toughness of the fabrication parts by FFF. They studied the effects of the infill density and build orientation of the printed chopped carbon fiber reinforced nylon (Onyx) and the printed unreinforced one, on the impact toughness property. The three different build orientations of A, B, and C according to Fig. 49(a), were considered. The samples were printed according to ISO 179 Plastics Determination of Charpy Impact Properties. The dimension of the prepared specimens was according to Fig. 49 (b). The printed specimens that were unnotched, were tested on a Ceast Impactor equipment located in TUBİTAK MAM at room temperature.

The nylon had better toughness in comparison with Onyx, about 2.5 times better. Also, the specimens, which received an impact in between two layers (A-Build Onyx 100%) had lower toughness (about 10 times) compared to specimens that received an impact, not between deposited layers (C-Build Onyx 100% and B-Build Onyx 100%). As for the effect of the infill density, by changing the infill density to 75%, the toughness decreased about 50%. However, by further infill density reduction by another 25% reduction to reach 50% infill density, the toughness reduced only less than 5% (Fig. 50). Generally, it was concluded that the impact toughness is a severe anisotropic property.

Carneiro et al. [60], studied on FFF process of polypropylene (PP). As a part of their research, they compared the tensile properties of PP and glass reinforced PP (GRPP). They indicated that the use of glass fibers as reinforcement was effective in the FFF process. It was reported that the modulus and strength of PP were increased about 30% and 40%, respectively, by the use of glass fibers as reinforcements.

The flow of reinforcements is an important aspect of the FFF process of composites. The flow of an 8vol. % carbon fiber reinforced epoxy through the tip of a nozzle was modeled by Lewicki et al. [61]. They considered the carbon fibers as discrete particles in the simulations. Therefore, fiber–fiber interactions and fiber-wall interactions were

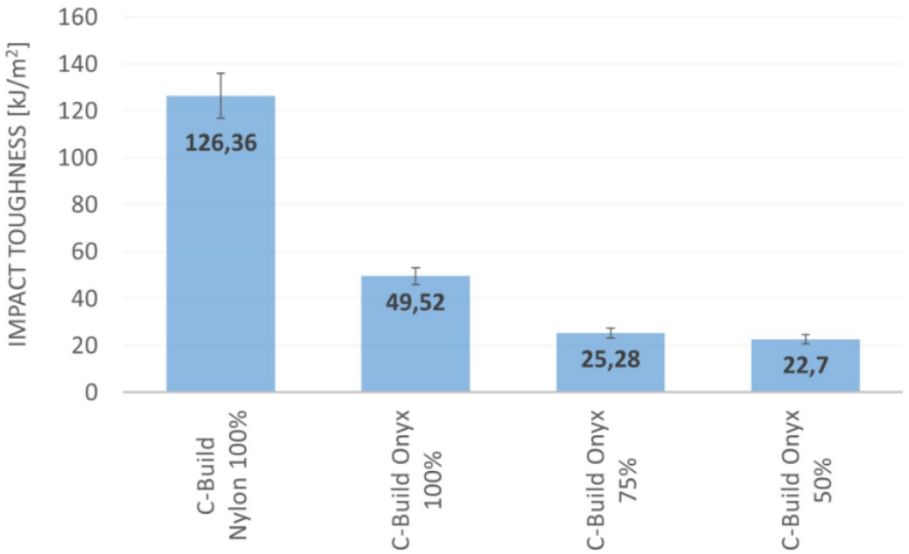


**Fig. 50** The Charpy impact toughness results of specimens built with different densities [59]

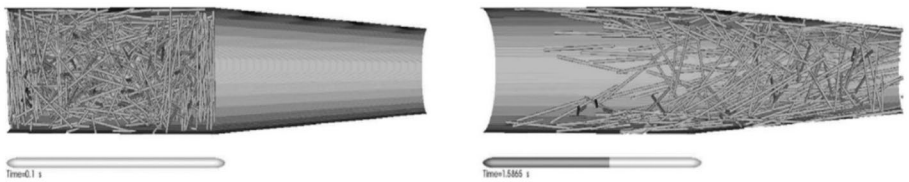

**Fig. 51** Fiber orientation evolution with time at a constant pressure [61]

taken into account. The fibers were considered as separate domains and particle–particle interactions were implemented with frictional, inelastic contact forces. Moreover, fluid dynamics equations have been used. Figure 51 demonstrates the orientation evolution of an initially randomly oriented arrangement of fibers.

Ankit Gupta et al. [62], studied the mechanical properties of the FFF manufactured polycarbonate reinforced with short carbon fiber (SCF) composite. The specimens were printed with different volume fractions of short carbon fibers (3%, 5%, 7.5%, 10%) and different printing speed values of 25, 50, and 75 mm/s. It was found out that the two selected variables, which were volume fractions of short carbon fibers and printing speed, affect the mechanical properties of the printed specimens, greatly.

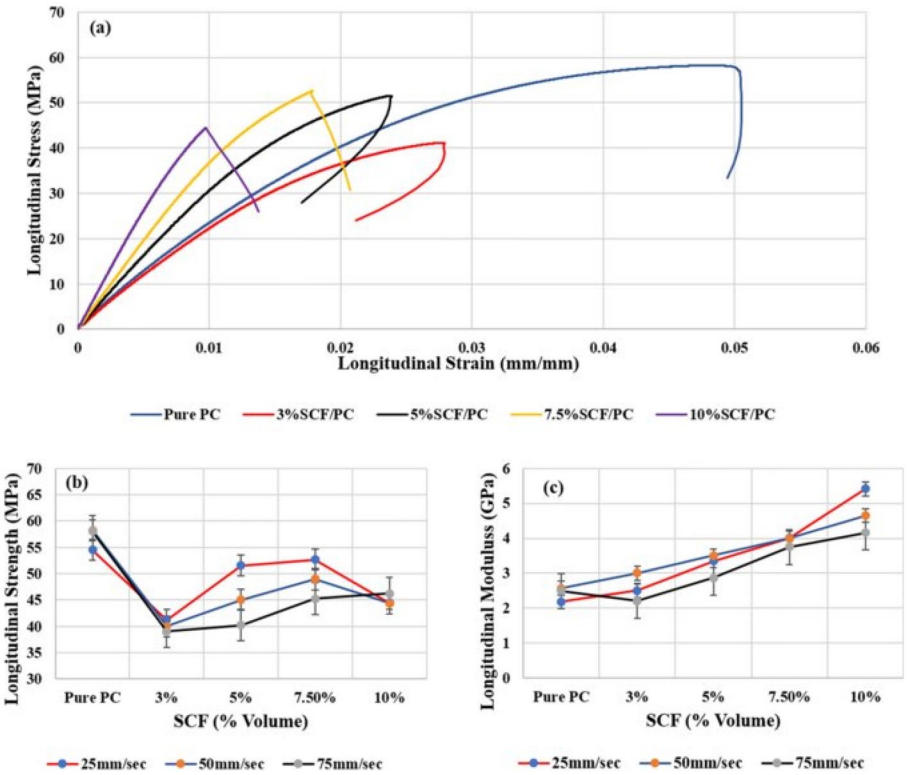


**Fig. 52** (**a**) Obtained longitudinal stress–strain curves for the different percentage of short carbon fiber reinforcement. (**b**) Reinforcement percentage effect on longitudinal strength at printing speed of (i) 25 mm/s, (ii) 50 mm/s, (iii) 75 mm/s. (**c**) Reinforcement percentage effect on longitudinal modulus at printing speed of (i) 25 mm/s, (ii) 50 mm/s, (iii) 75 mm/s [62]

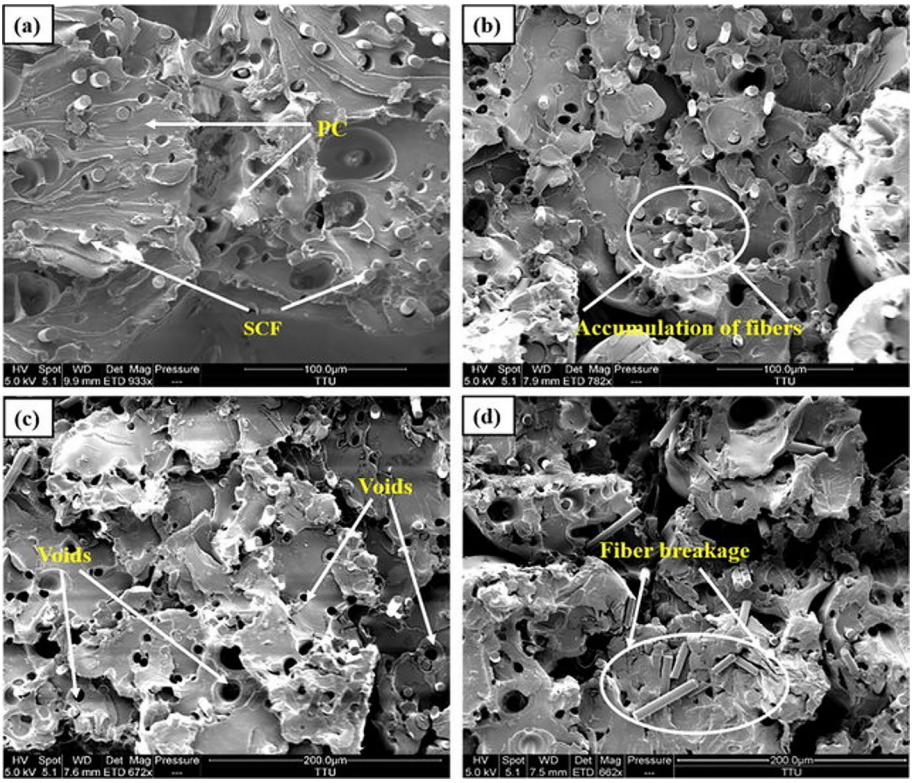


**Fig. 53** The obtained SEM images of the printed samples after tensile testing. (**a**) the distribution of fibers and matrix, (**b**) the observed accumulation of the short carbon fibers at one place. (**c**) short carbon fiber pull-out and d) short carbon fiber breakage at a high percentage [62]

It is stated that as the volume fraction of the used short carbon fiber reinforcement was increased, the suitable load transferring from polymer matrix to reinforcement was increased, up to 7.5% of reinforcement. Further increase amount (more than 7.5%) of the used short carbon fibers, didn't increase the tensile strength of the printed specimens anymore (the tensile strength decreased or become stable on a specific value), Fig. 52a.

As for the reason of the tensile strength decrease related to the printed specimens with more than 7.5% short carbon fibers (as reinforcement), the local accumulation of reinforcements (Fig. 53b) in the polymer matrix was introduced. It is stated that many locations were remained dry in the polymer matrix which resulted in decreasing the strength of the printed composite. Also, the observed fiber pullout (Fig. 53c) and fiber breakage (Fig. 53d) phenomena were increased more by the increase of short carbon fiber percentage, which caused the creation of more voids and the further decrease of the tensile strength. In addition, the pure polycarbonate exhibited more tensile strength in comparison with reinforced samples (printed composite materials). The lack of perfect alignment of the short carbon fibers as the used reinforcements were stated as the reason for this decreasing in strength.

Tables 9 and 10 present the summary of extracted mechanical data for discontinuous fiber systems loaded parallel and perpendicular to the printing direction, respectively.

**Table 9** Mechanical data for discontinuous fiber systems loaded parallel to the printing direction

| References | Materials | Tensile strength (MPa) | Tensile modulus (GPa) |
|---|---|---|---|
| Ninge et al. [46] | ABS/CF 3wt.% | 40.8 | 2.1 |
| | ABS/CF 5wt.% | 42 | 2.45 |
| | ABS/CF 7.5wt.% | 41.5 | 2.5 |
| | ABS/CF 10wt.% | 33.8 | 2.15 |
| | ABS/CF 15wt.% | 35 | 2.25 |
| Tekinalp et al. [57] | ABS/CF 10wt.% | 52 | 7.7 |
| | ABS/CF 20wt.% | 60 | 11.5 |
| | ABS/CF 30wt.% | 62 | 13.8 |
| | ABS/CF 40wt.% | 67 | 13.7 |
| Hill et al. [63] | ABS/CF 20wt.% | 66.8 | 8.4 |
| Kunc [64] | ABS/CF 13vol.% | 53 | 8.15 |
| Love et al. [58] | ABS/CF 13vol.% | 70.69 | 8.91 |
| Duty et al. [65] | ABS/CF 20wt.% | 65.7 | 11.9 |
| | ABS/GF 20wt.% | 54.3 | 5.7 |
| | ABS/GF 40wt.% | 51.2 | 10.8 |
| Duty et al. [66] | ABS/CF 20wt.% | 47.7 | 10.87 |
| | ABS/CF 15wt.% | 61.9 | 11.88 |
| | PEI/CF 20wt.% | 61.1 | 8.36 |
| Perez et al. [67] | ABS/Jute fiber 5wt.% | 25.9 | 1.54 |
| Shofner et al. [68] | ABS/VGCF 10wt.% | 37.4 | 0.8 |
| Ferreira et al. [69] | PLA/CF 15wt.% | 53.4 | 7.54 |
| Shofner et al. [70] | ABS/VGCF 5wt.% | 27 | 1.27 |
| | ABS/5wt.% SWNT | 32.5 | 1.74 |
| Compton and Lewis [71] | Epoxy/SiC/CF 10wt.% | 66.2 | 24.5 |
| Mahajan et al. [72] | Epoxy/CF 15wt.% | 66.3 | 4.05 |
| Gardner et al. [73] | PEI/CNT 4.7wt.% | 125.3 | 3 |
| DeNardo [74] | PPS/CF 50wt.% | 92.2 | 26.4 |

**Table 10** Mechanical data for discontinuous fiber-loaded perpendicular to the printing direction

| References | Materials | Tensile strength (MPa) | Tensile modulus (GPa) |
|---|---|---|---|
| Duty et al. [66] | ABS/chopped CF 20wt.% | 6.8 | 1.98 |
| | ABS/CF 15wt.% | 5.8 | 1.83 |
| | PEI/CF 20wt.% | 4.3 | 1.1 |
| Love et al. [58] | ABS/CF 13vol.% | 7 | 1.52 |
| DeNardo [74] | PPS/CF 50wt.% | 9.72 | 2.6 |
| Ferreira et al. [69] | PLA/CF 15wt.% | 35.4 | 3.92 |
| Mahajan et al. [72] | Epoxy/CF 15wt.% | 46 | 2.84 |
| Duty et al. [65] | ABS/CF 20wt.% | 10.3 | 2.1 |
| | ABS/GF 20wt.% | 15.3 | 2.5 |
| Compton [71] | Epoxy/SiC/CF 10wt.% | 43.9 | 8.06 |
| Hill et al. [63] | ABS/CF 20wt.% | 12.8 | 2.6 |
| Kunc [64] | ABS/CF 13vol.% | 13 | 2.2 |

In Tables 9 and 10, one can note that the difference in properties along and transverse to print direction due to short fiber alignment. The scattering in properties is due to processing conditions.

## 5 Conclusion

The present paper summarizes past published work on Fused Filament Fabrication (FFF) with fiber reinforced polymeric materials. Influencing parameters in the FFF process such as road width, print speed, layer thickness, feed rate and build temperature of the model (both liquefier and envelope temperature), fiber orientation, the layer position, volume fraction, and infill orientation have been studied. These parameters considered in the strength/bonding or physicochemical characterizations of FFF-fabricated parts have been presented in detail. An overview of mechanical properties of printed parts for different composite material systems is presented and discussed. Three types of reinforced polymers in the FFF process have been considered: powder reinforced polymers, continuous fiber-reinforced polymers, and short fiber reinforced polymers. This study covers the way for the development of a design support system for components printed with the FFF process. Indeed, the industrial world is using this technology more and more in the production of the complex small series parts. The knowledge produced by this article will help to better formalize methods and tools to optimize the design process of composite parts under different mechanical constraints.

## 6 Data Availability Statements

All data generated or analyzed during this study are included in this published article.

## References


1. Durgun, I., & Ertan, R.: Experimental investigation of FDM process for improvement of mechanical properties and production cost. Rapid Prototyp. J. (2014)
2. Górski, F., Kuczko, W.I.E.S.ŁA.W., Wichniarek, R.A.D.O.S.ŁA.W.: Impact strength of ABS parts manufactured using Fused Deposition Modeling technology. Archives of Mechanical Technology and Automation **31**(1), 3–12 (2014)
3. Baich, L., Manogharan, G., Marie, H.: Study of infill print design on production cost-time of 3D printed ABS parts. Int. J. Rapid Manuf. **5**(3–4), 308–319 (2015)
4. Górski, F., Wichniarek, R., Kuczko, W., Andrzejewski, J.: Experimental determination of critical orientation of ABS parts manufactured using fused deposition modelling technology. J. Mach. Eng. **15**(4), 121–132 (2015)
5. Cuan-Urquizo, E., Barocio, E., Tejada-Ortigoza, V., Pipes, R.B., Rodriguez, C.A., Roman-Flores, A.: Characterization of the mechanical properties of FFF structures and materials: A review on the experimental, computational and theoretical approaches. Materials **12**(6), 895 (2019)
6. Furlanello, F., Bertoldi, A., Dallago, M., Furlanello, C., Fernando, F., Inama, G., Chierchia, S.: Cardiac arrest and sudden death in competitive athletes with arrhythmogenic right ventricular dysplasia. Pacing Clin. Electrophysiol. **21**(1), 331–335 (1998)
7. Lee, B.H., Abdullah, J., Khan, Z.A.: Optimization of rapid prototyping parameters for production of flexible ABS object. J. Mater. Process. Technol. **169**(1), 54–61 (2005)
8. Sun, Q., Rizvi, G. M., Bellehumeur, C. T., & Gu, P.: Effect of processing conditions on the bonding quality of FDM polymer filaments. Rapid Prototyp. J. (2008)

9. Sood, A.K., Ohdar, R.K., Mahapatra, S.S.: Parametric appraisal of mechanical property of fused deposition modelling processed parts. Mater. Des. **31**(1), 287–295 (2010)
10. Fatimatuzahraa, A. W., Farahaina, B., & Yusoff, W. A. Y. (2011, September). The effect of employing different raster orientations on the mechanical properties and microstructure of Fused Deposition Modeling parts. In 2011 IEEE Symposium on Business, Engineering and Industrial Applications (ISBEIA) (pp. 22–27).
11. Croccolo, D., De Agostinis, M., Olmi, G.: Experimental characterization and analytical modelling of the mechanical behaviour of fused deposition processed parts made of ABS-M30. Comput. Mater. Sci. **79**, 506–518 (2013)
12. Mahmood, S., Qureshi, A. J., Goh, K. L., & Talamona, D.: Tensile strength of partially filled FFF printed parts: experimental results. Rapid Prototyp. J. (2017)
13. Raney, K., Lani, E., Kalla, D.K.: Experimental characterization of the tensile strength of ABS parts manufactured by fused deposition modeling process. Mater. Today: Proc. **4**(8), 7956–7961 (2017)
14. Harris, M., Potgieter, J., Archer, R., Arif, K.M.: Effect of material and process specific factors on the strength of printed parts in fused filament fabrication: A review of recent developments. Materials **12**(10), 1664 (2019)
15. Fodran, E, Martin K, and Unny M.: "Mechanical and dimensional characteristics of fused deposition modeling build styles." 1996 International Solid Freeform Fabrication Symposium. (1996)
16. Es-Said, O.S., Foyos, J., Noorani, R., Mendelson, M., Marloth, R., Pregger, B.A.: Effect of layer orientation on mechanical properties of rapid prototyped samples. Mater. Manuf. Process. **15**(1), 107–122 (2000)
17. Rodríguez, J. F., Thomas, J. P., & Renaud, J. E.: Mechanical behavior of acrylonitrile butadiene styrene (ABS) fused deposition materials. Experimental investigation. Rapid Prototyp. J. (2001)
18. Ahn, S. H., Montero, M., Odell, D., Roundy, S., & Wright, P. K.: Anisotropic material properties of fused deposition modeling ABS. Rapid Prototyp. J. (2002)
19. Sood, A.K., Ohdar, R.K., Mahapatra, S.S.: Experimental investigation and empirical modelling of FDM process for compressive strength improvement. J. Adv. Res. **3**(1), 81–90 (2012)
20. Ziemian, S., Okwara, M., & Ziemian, C. W.: Tensile and fatigue behavior of layered acrylonitrile butadiene styrene. Rapid Prototyp. J. (2015)
21. Onwubolu, G. C., & Rayegani, F.: Characterization and optimization of mechanical properties of ABS parts manufactured by the fused deposition modelling process. Int. J. Manuf. Eng. (2014)
22. Tymrak, B.M., Kreiger, M., Pearce, J.M.: Mechanical properties of components fabricated with open-source 3-D printers under realistic environmental conditions. Mat. Des. **58**, 242–246 (2014)
23. Ebel, E., & Sinnemann, T.: Fabrication of FDM 3D objects with ABS and PLA and determination of their mechanical properties. RTejournal (1) (2014)
24. Rankouhi, B., Javadpour, S., Delfanian, F., Letcher, T.: Failure analysis and mechanical characterization of 3D printed ABS with respect to layer thickness and orientation. J. Fail. Anal. Prev. **16**(3), 467–481 (2016)
25. Letcher, T., Rankouhi, B., & Javadpour, S.: Experimental study of mechanical properties of additively manufactured ABS plastic as a function of layer parameters. In ASME International Mechanical Engineering Congress and Exposition (Vol. 57359, p. V02AT02A018). Am. Soc. Mech. Eng. (2015, November)
26. Fernandez-Vicente, M., Calle, W., Ferrandiz, S., & Conejero, A.: Effect of infill parameters on tensile mechanical behavior in desktop 3D printing. 3D Print. Addit. Manuf. 3(3), 183–192 (2016)
27. Alvarez, C., K. L., Lagos C, R. F., & Aizpun, M. : Investigating the influence of infill percentage on the mechanical properties of fused deposition modelled ABS parts. Ingeniería e Investigación **36**(3), 110–116 (2016)
28. Hernandez, R., Slaughter, D., Whaley, D., Tate, J., & Asiabanpour, B.: Analyzing the tensile, compressive, and flexural properties of 3D printed ABS P430 plastic based on printing orientation using fused deposition modeling. In 27th Annual International Solid Freeform Fabrication Symposium, Austin, TX. 939–950 (2016)
29. Torrado, A.R., Roberson, D.A.: Failure analysis and anisotropy evaluation of 3D-printed tensile test specimens of different geometries and print raster patterns. J. Fail. Anal. Prev **16**(1), 154–164 (2016)
30. Cantrell, J. T., Rohde, S., Damiani, D., Gurnani, R., DiSandro, L., Anton, J., & Ifju, P. G.: Experimental characterization of the mechanical properties of 3D-printed ABS and polycarbonate parts. Rapid Prototyp. J. (2017)
31. Nikzad, M., Masood, S.H., Sbarski, I.: Thermo-mechanical properties of a highly filled polymeric composites for fused deposition modeling. Mater. Des. **32**(6), 3448–3456 (2011)

32. Hwang, S., Reyes, E.I., Moon, K.S., Rumpf, R.C., Kim, N.S.: Thermo-mechanical characterization of metal/polymer composite filaments and printing parameter study for fused deposition modeling in the 3D printing process. J. Electron. Mater. **44**(3), 771–777 (2015)
33. Isakov, D.V., Lei, Q., Castles, F., Stevens, C.J., Grovenor, C.R.M., Grant, P.S.: 3D printed anisotropic dielectric composite with meta-material features. Mater. Des. **93**, 423–430 (2016)
34. Shemelya, C.M., Rivera, A., Perez, A.T., Rocha, C., Liang, M.I.N., Yu, X., Wicker, R.B.: Mechanical, electromagnetic, and X-ray shielding characterization of a 3D printable tungsten–polycarbonate polymer matrix composite for space-based applications. J. Electron. Mater. **44**(8), 2598–2607 (2015)
35. Boparai, K., Singh, R., Singh, H.: Comparison of tribological behaviour for Nylon6-Al-Al2O3 and ABS parts fabricated by fused deposition modelling: This paper reports a low cost composite material that is more wear-resistant than conventional ABS. Virtual Phys. Prototy. **10**(2), 59–66 (2015)
36. Matsuzaki, R., Ueda, M., Namiki, M., Jeong, T.K., Asahara, H., Horiguchi, K., Hirano, Y.: Three-dimensional printing of continuous-fiber composites by in-nozzle impregnation. Sci. Rep. **6**, 23058 (2016)
37. Hao, W., Liu, Y., Zhou, H., Chen, H., Fang, D.: Preparation and characterization of 3D printed continuous carbon fiber reinforced thermosetting composites. Polym. Test. **65**, 29–34 (2018)
38. Li, N., Li, Y., Liu, S.: Rapid prototyping of continuous carbon fiber reinforced polylactic acid composites by 3D printing. J. Mater. Process. Technol. **238**, 218–225 (2016)
39. Tian, X., Liu, T., Yang, C., Wang, Q., Li, D.: Interface and performance of 3D printed continuous carbon fiber reinforced PLA composites. Compos. A: Appl. Sci. Manuf. **88**, 198–205 (2016)
40. Hao, W., Yuan, Y., Zhu, J., Chen, L.: Effect of impact damage on the curved beam interlaminar strength of carbon/epoxy laminates. J. Adhes Sci. Technol. **30**(11), 1189–1200 (2016)
41. Akhoundi, B., Behravesh, A.H., Bagheri Saed, A.: Improving mechanical properties of continuous fiber-reinforced thermoplastic composites produced by FDM 3D printer. J. Reinf Plast. Compos. **38**(3), 99–116 (2019)
42. Van Der Klift, F., Koga, Y., Todoroki, A., Ueda, M., Hirano, Y., Matsuzaki, R.: 3D printing of continuous carbon fibre reinforced thermo-plastic (CFRTP) tensile test specimens. Open J. Compos. Mater. **6**(01), 18 (2016)
43. Agarwal, K., Kuchipudi, S.K., Girard, B., Houser, M.: Mechanical properties of fiber reinforced polymer composites: A comparative study of conventional and additive manufacturing methods. J. Compos.Mater. **52**(23), 3173–3181 (2018)
44. Oztan, C., Karkkainen, R., Fittipaldi, M., Nygren, G., Roberson, L., Lane, M., Celik, E.: Microstructure and mechanical properties of three dimensional-printed continuous fiber composites. J. Compos. Mater. **53**(2), 271–280 (2019)
45. Dong, G., Tang, Y., Li, D., Zhao, Y.F.: Mechanical properties of continuous kevlar fiber reinforced composites fabricated by fused deposition modeling process. Procedia Manuf. **26**, 774–781 (2018)
46. Ning, F., Cong, W., Qiu, J., Wei, J., Wang, S.: Additive manufacturing of carbon fiber reinforced thermoplastic composites using fused deposition modeling. Compos. Part B Eng. **80**, 369–378 (2015)
47. van de Werken, N., Hurley, J., Khanbolouki, P., Sarvestani, A.N., Tamijani, A.Y., Tehrani, M.: Design considerations and modeling of fiber reinforced 3D printed parts. Compos. Part B Eng. **160**, 684–692 (2019)
48. N. Sarvestani, A., van de Werken, N., Khanbolouki, P., & Tehrani, M.: 3D printed composites with continuous carbon fiber reinforcements. In ASME International Mechanical Engineering Congress and Exposition (Vol. 58356, p. V002T02A031). American Society of Mechanical Engineers. (2007, November)
49. Chen, Y., Rios, C.O., Imeri, A., Russell, N.A., Fidan, I.: Investigation of the tensile properties in fibre-reinforced additive manufacturing and fused filament fabrication. Int. J. Rapid Manuf. **9**(2–3), 251–267 (2020)
50. Imeri, A., Fidan, I., Allen, M., Perry, G.: Effect of fiber orientation in fatigue properties of FRAM components. Procedia Manuf. **26**, 892–899 (2018)
51. Dickson, A.N., Barry, J.N., McDonnell, K.A., Dowling, D.P.: Fabrication of continuous carbon, glass and Kevlar fibre reinforced polymer composites using additive manufacturing. Addit. Manuf. **16**, 146–152 (2017)
52. Chuncheng, Y.: 3D printing for continuous fiber reinforced thermoplastic composites: mechanism and performance. Rapid Prototyp. J. **23**(1), 209–215 (2017)
53. Tian, X., Liu, T., Wang, Q., Dilmurat, A., Li, D., Ziegmann, G.: Recycling and remanufacturing of 3D printed continuous carbon fiber reinforced PLA composites. J. Clean. Prod. **142**, 1609–1618 (2017)
54. Melenka, G.W., Cheung, B.K., Schofield, J.S., Dawson, M.R., Carey, J.P.: Evaluation and prediction of the tensile properties of continuous fiber-reinforced 3D printed structures. Composite Structures **153**, 866–875 (2016)

55. Bettini, P., Alitta, G., Sala, G., Di Landro, L.: Fused deposition technique for continuous fiber reinforced thermoplastic. J. Mater. Eng. Perform. **26**(2), 843–848 (2017)
56. Zhong, W., Li, F., Zhang, Z., Song, L., Li, Z.: Short fiber reinforced composites for fused deposition modeling. Mater. Sci. Eng. A **301**(2), 125–130 (2001)
57. Tekinalp, H.L., Kunc, V., Velez-Garcia, G.M., Duty, C.E., Love, L.J., Naskar, A.K., Ozcan, S.: Highly oriented carbon fiber–polymer composites via additive manufacturing. Compos. Sci. Technol. **105**, 144–150 (2014)
58. Love, L.J., Kunc, V., Rios, O., Duty, C.E., Elliott, A.M., Post, B.K., Blue, C.A.: The importance of carbon fiber to polymer additive manufacturing. J. Mater. Res. **29**(17), 1893 (2014)
59. Yasa, E.: Anisotropicimpact toughnness of chopped carbon fiber reinforced nylon fabricated bymaterial-extrusion-based additive manufacturing. Anadolu University of Sciences & Technology-A: Applied Sciences & Engineering, **20**(2) (2019)
60. Carneiro, O.S., Silva, A.F., Gomes, R.: Fused deposition modeling with polypropylene. Mater. Des. **83**, 768–776 (2015)
61. Lewicki, J.P., Rodriguez, J.N., Zhu, C., Worsley, M.A., Wu, A.S., Kanarska, Y., Hensleigh, R.: 3D-printing of meso-structurally ordered carbon fiber/polymer composites with unprecedented orthotropic physical properties. Sci. Rep. **7**(1), 1–14 (2017)
62. Gupta, A., Fidan, I., Hasanov, S., Nasirov, A.: Processing, mechanical characterization, and micrography of 3D-printed short carbon fiber reinforced polycarbonate polymer matrix composite material. Int. J. Adv. Manuf. Technol. **107**(7), 3185–3205 (2020)
63. Hill, C., Rowe, K., Bedsole, R., Earle, J., & Kunc, V.: Materials and process development for direct digital manufacturing of vehicles. In SAMPE Long Beach 2016 Conference and Exhibition. (2016, May)
64. Kunc, V. (2015, September). Advances and challenges in large scale polymer additive manufacturing. In Proceedings of the 15th SPE Automotive Composites Conference, Novi, MI, USA **9** (2015)
65. Duty, C. E., Drye, T., & Franc, A.: Material development for tooling applications using big area additive manufacturing (BAAM) (No. ORNL/TM-2015/78). Oak Ridge National Lab.(ORNL), Oak Ridge, TN (United States). Manufacturing Demonstration Facility (MDF) (2015)
66. Duty, C. E., Kunc, V., Compton, B., Post, B., Erdman, D., Smith, R., & Love, L.: Structure and mechanical behavior of Big Area Additive Manufacturing (BAAM) materials. Rapid Prototyp. J. (2017)
67. Perez, A.R.T., Roberson, D.A., Wicker, R.B.: Erratum to: Fracture surface analysis of 3D-printed tensile specimens of novel ABS-based materials. J. Fail. Anal. Prev. **14**(4), 549–549 (2014)
68. Shofner, M.L., Lozano, K., Rodríguez-Macías, F.J., Barrera, E.V.: Nanofiber-reinforced polymers prepared by fused deposition modeling. J. Appl. Polym. Sci. **89**(11), 3081–3090 (2003)
69. Ferreira, R.T.L., Amatte, I.C., Dutra, T.A., Bürger, D.: Experimental characterization and micrography of 3D printed PLA and PLA reinforced with short carbon fibers. Compos. Part B Eng. **124**, 88–100 (2017)
70. Shofner, M. L., Rodriguez-Macias, F. J., Vaidyanathan, R., and Barrera, E. V.: "Single wall nanotube and vapor grown carbon fiber reinforced polymers processed by extrusion freeform fabrication," Composites, Part A **34**(12), 1207–1217 (2003)
71. Compton, B.G., Lewis, J.A.: 3D-printing of lightweight cellular composites. Adv. Mater. **26**(34), 5930–5935 (2014)
72. Mahajan, C., & Cormier, D.: 3D printing of carbon fiber composites with preferentially aligned fibers. In IIE annual conference. Proceedings (p. 2953). Institute of Industrial and Systems Engineers (IISE). (2015)
73. Gardner, J. M., Sauti, G., Kim, J. W., Cano, R. J., Wincheski, R. A., Stelter, C. J., & Siochi, E. J.: Additive manufacturing of multifunctional components using high density carbon nanotube yarn filaments. (2016)
74. DeNardo, N. M.: Additive manufacturing of carbon fiber-reinforced thermoplastic composites. (2016)